

Branch cuts of Stokes wave on deep water. Part II: Structure and location of branch points in infinite set of sheets of Riemann surface

Pavel M. Lushnikov[†]

Department of Mathematics and Statistics, University of New Mexico, Albuquerque, MSC01
1115, NM, 87131, USA

(Received 30 June 2016)

Stokes wave is a finite amplitude periodic gravity wave propagating with constant velocity in inviscid fluid. Complex analytical structure of Stokes wave is analyzed using a conformal mapping of a free fluid surface of Stokes wave into the real line with fluid domain mapped into the lower complex half-plane. There is one square root branch point per spatial period of Stokes located in the upper complex half-plane at the distance v_c from the real axis. The increase of Stokes wave height results in approaching v_c to zero with the limiting Stokes wave formation at $v_c = 0$. The limiting Stokes wave has $2/3$ power law singularity forming $2\pi/3$ radians angle on the crest which is qualitatively different from the square root singularity valid for arbitrary small but nonzero v_c making the limit of zero v_c highly nontrivial. That limit is addressed by crossing a branch cut of a square root into the second and subsequently higher sheets of Riemann surface to find coupled square root singularities at the distances $\pm v_c$ from the real axis at each sheet. The number of sheets is infinite and the analytical continuation of Stokes wave into all these sheets is found together with the series expansion in half-integer powers at singular points within each sheet. It is conjectured that non-limiting Stokes wave at the leading order consists of the infinite number of nested square root singularities which also implies the existence in the third and higher sheets of the additional square root singularities away from the real and imaginary axes. These nested square roots form $2/3$ power law singularity of the limiting Stokes wave as v_c vanishes.

Key words: Surface gravity waves; Stokes wave; Complex singularities of two-dimensional fluid flows; Free surface flows

1. Introduction

In Part I (Dyachenko *et al.* 2016), we obtained Stokes wave solution numerically with high precision and analyzed that solution using Padé approximation. We showed a convergence of Padé approximation of Stokes wave to a single branch cut per spatial period in the upper complex half plane \mathbb{C}^+ of the axillary complex variable w . In this paper we formulate the nonlinear integral equation for the jump of Stokes wave at the branch cut in the physical (first) sheet of Riemann surface. We show that the Riemann surface of Stokes has infinite number of sheets as sketched in Figure 1 and study the structure of singularities in these sheets.

[†] Email address for correspondence: plushnik@math.unm.edu

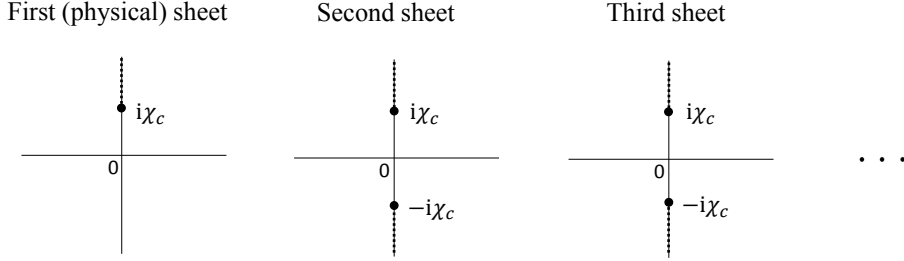


FIGURE 1. A schematic of Riemann surface sheets for non-limiting Stokes wave in the complex variable ζ (1.6) near the origin. The first (physical) sheet has a single square root singularity at $\zeta = i\chi_c$ in the upper complex half-plane \mathbb{C}^+ with the the lower complex half-plane \mathbb{C}^- corresponding to the domain occupied by the fluid. Other (non-physical) sheets have square root singularities at $\zeta = \pm i\chi_c$. Dashed lines show branch cuts. In addition there are the singularities at $\zeta = \pm i$ in all sheets which corresponds to $w = \infty$. As well as starting from the third sheet there are square root singularities away from both real and imaginary axes at the distances more that several times exceeding χ_c , i.e. well beyond the disks of convergence $|\zeta \pm i\chi_c| < 2\chi_c$.

Stokes wave is the fully nonlinear periodic gravity wave propagating with the constant velocity c (Stokes 1847, 1880*a*). It corresponds to two-dimensional potential flow of an ideal incompressible fluid with free surface. Following Part I (Dyachenko *et al.* 2016), we use scaled units at which $c = 1$ for the linear gravity waves and the spatial period is $\lambda = 2\pi$. Nonlinearity of Stokes wave increases with the increase of H/λ , where H is the Stokes wave height which is defined as the vertical distance from the crest to the trough of Stokes wave. Stokes wave has $c > 1$ and the limit $H \rightarrow 0$, $c \rightarrow 1$ corresponds to the linear gravity wave. The Stokes wave of the greatest height $H = H_{max}$ (also called by the limiting Stokes wave) has the singularity in the form of the sharp angle of $2\pi/3$ radians on the crest (Stokes 1880*b*). We assume that singularity of the limiting Stokes wave touches the fluid surface at $w = 0$ and corresponds the following expansion

$$z(w) = i\frac{c^2}{2} - i\left(\frac{3c}{2}\right)^{2/3} (iw)^{2/3} + \text{h.o.t.} \quad (1.1)$$

which ensures the sharp angle of $2\pi/3$ radians on the crest. Equation (1.1) recovers the result of Stokes (1880*b*). Here h.o.t. means higher order terms which approaches 0 faster than $w^{2/3}$ as $w \rightarrow 0$. Also

$$z(w) = x(w) + iy(w) \quad (1.2)$$

is the conformal transformation which maps a half-strip $-\pi \leq u \leq \pi$, $-\infty < v \leq 0$ of the conformal variable

$$w = u + iv \quad (1.3)$$

into a fluid domain of infinite depth $-\infty < y \leq \eta(x)$, $-\pi \leq x \leq \pi$ of the complex plane z (see Figure 1 of Part I (Dyachenko *et al.* 2016)). Here x and y are the horizontal and vertical physical coordinates, respectively. $y = \eta(x)$ is the surface elevation in the reference frame moving with the speed c . As discussed in details in Part I, choosing

$$z(w) = w + \tilde{z}(w), \quad (1.4)$$

with $x(w) = u + \tilde{x}(w)$ and $\tilde{y}(w) = v + y(w)$, ensures that $\tilde{z}(w)$ is 2π -periodic function

$$\tilde{z}(w + 2\pi) = \tilde{z}(w), \quad \tilde{x}(\pm\pi) = 0. \quad (1.5)$$

It was found by Grant (1973) that the corner singularity (1.1) might not be a simple algebraic branch point because next order term in the expansion (1.1) might be a power of the transcendental number. Rigorous results on the asymptotics near the crest of the limiting wave were found in Refs. Amick & Fraenkel (1987); McLeod (1987). These results were used in Refs. Fraenkel (2007, 2010); Fraenkel & Harwin (2010) to construct the exact bounds on the limiting Stokes wave and prove the local uniqueness using Banach's contraction mapping principle. More exact bounds were provided in Ref. Tanveer (2013). However, the question if log terms in the asymptotic expansion are possible in addition to the transcendental power asked in Ref. Amick & Fraenkel (1987) remains open. The existence of limiting Stokes wave with the jump of the slope at the crest in $2\pi/3$ radians was independently proven by Plotnikov (1982) and Amick *et al.* (1982).

In this paper we focus on analyzing singularities of near-limiting Stokes wave. Grant (1973) showed that assuming that singularity is a power law branch point, then that singularity has to have a square root form to the leading order. Tanveer (1991) provided much stronger result proving that the only possible singularity in the finite complex upper half-plane is of square root type. Ref. Plotnikov & Toland (2002) discusses the existence of a unique square root singularity above crests. The existence of only one square root singularity per period in a finite physical complex plane was also confirmed in Ref. (Dyachenko *et al.* 2013a) and Part I (Dyachenko *et al.* 2016) by analyzing the numerical solution for Stokes wave.

We now consider an additional conformal transformation between the complex plane $w = u + iv$ and the complex plane for the new variable

$$\zeta = \tan\left(\frac{w}{2}\right) \quad (1.6)$$

which maps the strip $-\pi < Re(w) < \pi$ into the complex ζ plane. In particular, the line segment $-\pi < w < \pi$ of the real line $w = u$ maps into the entire real line $(-\infty, \infty)$ in the complex ζ -plane as shown in Figure 5 of Part I (Dyachenko *et al.* 2016). Vertical half-lines $w = \pm\pi + iv$, $0 < v < \infty$ are mapped into a branch cut $i < \zeta < i\infty$. In a similar way, vertical half-lines $w = \pm\pi + iv$, $-\infty < v < 0$ are mapped into a branch cut $-i\infty < \zeta < -i$. However, 2π -periodicity of $\tilde{z}(w)$ (1.5) allows to ignore these two branch cuts because $\tilde{z}(w)$ is continuous across them. Complex infinities $w = \pm i\infty$ are mapped into $\zeta = \pm i$. An unbounded interval $[iv_c, i\infty)$, $v_c > 0$ is mapped into a finite interval $[i\chi_c, i)$ with

$$\chi_c = \tanh \frac{v_c}{2}. \quad (1.7)$$

The transformation (1.6) takes care of 2π -periodicity of Stokes wave so that the function $z(\zeta)$ defined in the complex plane $\zeta \in \mathbb{C}$ corresponds to the function $z(w)$ defined in the strip $-\pi < Re(w) = u < \pi$. Here and below we abuse notation and use the same symbol z for both functions of ζ and w (and similar for other symbols). The additional advantage of using the mapping (1.6) is the compactness of the interval $(i\chi_c, i)$ as mapped from the infinite interval $(iv_c, i\infty)$. Note that the mapping (1.6) is different from the commonly used (see e.g. Schwartz (1974); Tanveer (1991); Williams (1981)) mapping $\zeta = \exp(-iw)$ (maps the strip $-\pi \leq Re(w) < \pi$ into the unit circle). That exponential map leaves the interval $(iv_c, i\infty)$ infinite in ζ plane.

The main result of this paper is that it was found an infinite number of sheets of Riemann surface with square root branch points located at $\zeta = \pm i\chi_c$ starting from the second sheet (the first sheet has the singularity only at $\zeta = i\chi_c$). At each sheet (except the first one) these singularities are coupled through complex conjugated terms which appear in the equation for Stokes wave. In contrast, the only singularity at $\zeta = i\chi_c$ of the

first sheet (besides the singularity at $\zeta = i$) does not have a complex conjugated sister at $\zeta = -i\chi_c$ which makes that (physical) sheet distinct from all others. It is conjectured that the leading order form of non-limiting Stokes wave has the form of the infinite number of nested square root singularities. These nested square roots form 2/3 power law singularity of the limiting Stokes wave as $\chi_c \rightarrow 0$.

The paper is organized as follows. In Section 2 a closed nonlinear integral equation for Stokes wave in terms of the density (jump) at the branch cut is derived and the numerical method to solve that integral equation is given. Section 3 provides an alternative form for the equation of Stokes wave. Section 4 uses that alternative form to find an asymptotic of both Stokes wave at $Im(w) \rightarrow +\infty$ and the jump at the branch cut. Section 5 discusses a numerical procedure to analyze the structure of sheets of Riemann surface for Stokes wave by the integration of the corresponding nonlinear ordinary differential equation (ODE) in the complex plane. Section 6 derives the analytical expressions for coupled series expansions at $\zeta = \pm i\chi_c$ to reveal the structure of Riemann surface for Stokes wave. Section 7 analyzes possible singularities of Stokes in all sheets of Riemann surface and concludes that the only possible singularity for finite value of w is the square root branch point. Section 8 provides a conjecture on recovering of 2/3 power law of limiting Stokes wave from an infinite number of nested square root singularities of non-limiting Stokes wave in the limit $\chi_c \rightarrow 0$. In Section 9 the main results of the paper are discussed. Appendix A shows the equivalence of two forms of equation for Stokes wave used in the main text. Appendix B relates different forms of equation for Stokes wave in the rest frame and in the moving frame. Appendix C provides tables of the numerical parameters of Stokes wave.

2. Closed integral equation for Stokes wave through the density at the branch cut

The equation for Stokes wave was derived in Ref. Zakharov & Dyachenkov (1996) and Part I (Dyachenko *et al.* 2016) from Euler's equations for the potential flow of ideal fluid with free surface (see also Appendices A and B). That equation is defined at the real line $w = u$ and takes the following form

$$-c^2 y_u + y y_u + \hat{H}[y(1 + \tilde{x}_u)] = 0, \quad (2.1)$$

where

$$\hat{H}f(u) = \frac{1}{\pi} \text{p.v.} \int_{-\infty}^{+\infty} \frac{f(u')}{u' - u} du' \quad (2.2)$$

is the Hilbert transform with p.v. meaning a Cauchy principal value of integral and subscripts in t and u mean partial derivatives here and further. The Hilbert operator \hat{H} transforms into the multiplication operator

$$(\hat{H}f)_k = i \text{sign}(k) f_k, \quad (2.3)$$

for the Fourier coefficients (harmonics) f_k ,

$$f_k = \frac{1}{2\pi} \int_{-\pi}^{\pi} f(u) \exp(-iku) du, \quad (2.4)$$

of the periodic function $f(u) = f(u + 2\pi)$ represented through the Fourier series

$$f(u) = \sum_{k=-\infty}^{\infty} f_k \exp(iku). \quad (2.5)$$

Here $\text{sign}(k) = -1, 0, 1$ for $k < 0$, $k = 0$ and $k > 0$, respectively. Equation (2.5) implies that

$$\hat{H}^2 f = -(f - f_0), \quad (2.6)$$

where f_0 is the zeroth Fourier harmonic of f .

It is convenient to decompose the Fourier series (2.5) as follows

$$f(u) = f^+(u) + f^-(u) + f_0, \quad (2.7)$$

where

$$f^+(w) = \sum_{k=1}^{\infty} f_k \exp(ikw) \quad (2.8)$$

is the analytical function in \mathbb{C}^+ and

$$f^-(w) = \sum_{k=-\infty}^{-1} f_k \exp(ikw) \quad (2.9)$$

is the analytical function in the lower complex half-plane \mathbb{C}^- . Then equation (2.3) implies that

$$\hat{H} f = i(f^+ - f^-). \quad (2.10)$$

Also using equation (2.3) we define the operator,

$$\hat{P} = \frac{1}{2}(1 + i\hat{H}), \quad (2.11)$$

projecting any 2π -periodic function f into a function which has analytical continuation from the real line $w = u$ into \mathbb{C}^- as follows

$$\hat{P} f = f^- + \frac{f_0}{2}. \quad (2.12)$$

One can apply \hat{H} to (2.1) to obtain the following closed expression for y ,

$$\left(c^2 \hat{k} - 1\right) y - \left(\frac{\hat{k} y^2}{2} + y \hat{k} y\right) = 0, \quad (2.13)$$

where $\hat{k} \equiv -\partial_u \hat{H} = \sqrt{-\nabla^2}$ and we used the following relations

$$y_u = \hat{H} \tilde{x}_u \quad \text{and} \quad \tilde{x}_u = -\hat{H} y_u, \quad (2.14)$$

which are valid for the analytic function $\tilde{z}_u(w)$ satisfying the decaying condition $\tilde{z}_u(w) \rightarrow 0$ as $v \rightarrow -\infty$. We also assume in deriving equation (2.13) from equation (2.1) that

$$\int_{-\pi}^{\pi} \eta(x) dx = \int_{-\pi}^{\pi} y(u) x_u(u) du = 0, \quad (2.15)$$

meaning that the mean elevation of the free surface is set to zero. Equation (2.15) reflects a conservation of the total mass of fluid. Equation (2.13) was derived in Ref. Babenko (1987) and later was independently obtained from results of Ref. Dyachenko *et al.* (1996)

in Dyachenko *et al.* (2013a). See also Ref. Zakharov & Dyachenkov (1996) for somewhat similar equation. Ref. Babenko (1987) and subsequent developments in Refs. Buffoni *et al.* (2000); Buffoni & Toland (2001); Plotnikov (1991); Shargorodsky & Toland (2008) used equation of the type (2.13) for the analysis of bifurcations.

Equation (2.13) is convenient for numerical simulation of Stokes wave because it depends on y only as detailed in Part I (Dyachenko *et al.* 2016). The operator \hat{k} is the multiplication operator in Fourier domain which is straightforward to evaluate numerically using Fast Fourier Transform.

In this paper it is however more convenient for analytical study to rewrite equation for Stokes wave in terms of the complex variable \tilde{z} . For that we apply the projector operator \hat{P} (2.11) to equation (2.1) which results in

$$c^2 \tilde{z}_u = -i\hat{P}[(\tilde{z} - \bar{\tilde{z}})(1 + \tilde{z}_u)], \quad (2.16)$$

where $\bar{f}(u) \equiv \bar{f}$ means complex conjugation of the function $f(u)$. Note that the complex conjugation $\bar{f}(w)$ of $f(w)$ in this paper is understood as applied with the assumption that $f(w)$ is the complex-valued function of the real argument w even if w takes the complex values so that

$$\bar{f}(w) \equiv \overline{f(\bar{w})}. \quad (2.17)$$

That definition ensures the analytical continuation of $f(w)$ from the real axis $w = u$ into the complex plane of $w \in \mathbb{C}$ and similar for functions of $\zeta \in \mathbb{C}$. If the function $f(w)$ is analytic in \mathbb{C}^- then $\bar{f}(w)$ is analytic in \mathbb{C}^+ as also follows from equations (2.7)-(2.9).

A numerical convergence of Padé approximation to the continuous density $\rho(\chi)$ of the branch cut was shown in Part I (Dyachenko *et al.* 2016) together with the parametrization of the branch cut of Stokes wave as follows

$$\tilde{z}(\zeta) = iy_b + \int_{\chi_c}^1 \frac{\rho(\chi')d\chi'}{\zeta - i\chi'}, \quad (2.18)$$

where $y_b \equiv y(u)|_{u=\pm\pi} \in \mathbb{R}$ is the minimum height of Stokes wave as a function of x (or in the similar way as the function of u). The density $\rho(\chi)$ is related to the jump Δ_{jump} of $\tilde{z}(\zeta)$ for crossing the branch cut at $\zeta = i\chi$ in counterclockwise direction as follows

$$\tilde{\Delta}_{jump} \equiv z(\zeta)|_{\zeta=i\chi-0} - \tilde{z}(\zeta)|_{\zeta=i\chi+0} = -2\pi\rho(\chi), \quad (2.19)$$

see also Part I (Dyachenko *et al.* 2016) for more details on that. We now use the parametrization (2.18) to study the Stokes wave equation (2.16). We eliminate the constant iy_b at $\zeta = \infty$ in (2.18) by introducing a new function

$$f(u) = \tilde{z}(u) - iy_b = \int_{\chi_c}^1 \frac{\rho(\chi')d\chi'}{\zeta - i\chi'}. \quad (2.20)$$

together with the complex conjugate

$$\bar{f}(u) = \int_{\chi_c}^1 \frac{\rho(\chi')d\chi'}{\zeta + i\chi'} \quad (2.21)$$

which was evaluated using the definition (2.17).

Equation (2.16) in the new valuable (2.20) takes the following form

$$-ic^2 f_u + iy_b + 2iy_b f_u + ff_u + \hat{P}f - \hat{P}\bar{f} - \hat{P}[f\bar{f}_u] = 0 \quad (2.22)$$

with f and \bar{f} given by equations (2.20) and (2.21), respectively.

2.1. Projection in ζ plane

The projector \hat{P} (2.11) is defined in terms of the independent variable u . Using equation (2.22) together with the definition (2.20) suggests to switch from u into the independent variable ζ . To identify how to compute \hat{P} in complex ζ -plane, we start from the Fourier series (2.4), (2.7) in variable u and make a change of variable (1.6) (assuming that $-\pi \leq u \leq \pi$ and $\zeta \in \mathbb{R}$) as follows

$$f(u) = f(\zeta) = \sum_{k=-\infty}^{\infty} f_n e^{iku} = \sum_{k=-\infty}^{\infty} f_n \exp[2ik \arctan \zeta] = \sum_{n=-\infty}^{\infty} f_k \left(\frac{\zeta - i}{\zeta + i} \right)^k (-1)^k, \quad (2.23)$$

where we abuse notation by assuming that $\tilde{f}(\zeta) \equiv f(u)$ and removing \sim sign. Equations (2.11), (2.12) and (2.23) imply that \hat{P} removes all Fourier harmonics with positive n and replaces the zeroth harmonic f_0 by $f_0/2$ as follows

$$\begin{aligned} \hat{P}f(u) &= \sum_{n=-\infty}^{\infty} f_k \hat{P}e^{iku} = \frac{f_0}{2} + \sum_{k=-\infty}^{-1} f_k \exp[ik2 \arctan \zeta] \\ &= \frac{f_0}{2} + \sum_{n=-\infty}^{-1} f_k \left(\frac{\zeta - i}{\zeta + i} \right)^k (-1)^k. \end{aligned} \quad (2.24)$$

Consider a particular case $f(u) = \frac{1}{\zeta - i\chi}$, $\chi \in \mathbb{R}$ and $\chi \neq 0$. We calculate f_k by equation (2.4) and (2.23) through the change of variable (1.6) implying $du = \frac{2}{\zeta^2 + 1} d\zeta$ as follows

$$f_{-k} = \frac{1}{2\pi} \int_{-\pi}^{\pi} f(u) e^{iku} du = \frac{1}{2\pi} \int_{-\infty}^{\infty} \frac{1}{\zeta - i\chi} \left(\frac{\zeta - i}{\zeta + i} \right)^k (-1)^k \frac{2}{\zeta^2 + 1} d\zeta. \quad (2.25)$$

Assuming $k \geq 0$ and closing the complex integration contour in the upper half-plane of ζ we obtain that

$$f_{-k} = i \left(\frac{\chi - 1}{\chi + 1} \right)^k (-1)^k \frac{2}{-\chi^2 + 1} \theta(\chi) + \delta_{k,0} \frac{1}{i - i\chi}. \quad (2.26)$$

For the zeroth harmonic f_0 , equation (2.26) results in

$$f_0 = \frac{i \operatorname{sign}(\chi)}{1 + \chi \operatorname{sign}(\chi)}, \quad (2.27)$$

where $\operatorname{sign}(\chi) = 1$ for $\chi > 0$ and $\operatorname{sign}(\chi) = -1$ for $\chi < 0$.

Using now equations (2.24), (2.26) and (2.27) we find that

$$\begin{aligned} \hat{P} \frac{1}{\zeta - i\chi} &= \frac{-i \operatorname{sign}(\chi)}{2[1 + \chi \operatorname{sign}(\chi)]} + \sum_{k=0}^{\infty} \left[i \left(\frac{\chi - 1}{\chi + 1} \right)^k (-1)^k \frac{2}{-\chi^2 + 1} \theta(\chi) + \delta_{k,0} \frac{1}{i - i\chi} \right] \\ &\quad \times \left(\frac{\zeta + i}{\zeta - i} \right)^k (-1)^k = \frac{1}{\zeta - i\chi} \theta(\chi) + \frac{1}{i - i\chi} \theta(-\chi) - \frac{i \operatorname{sign}(\chi)}{2[1 + \chi \operatorname{sign}(\chi)]}, \end{aligned} \quad (2.28)$$

where $\theta(\chi) = 1$ for $\chi > 0$ and $\theta(\chi) = 0$ for $\chi < 0$.

In a similar way, for $f(\zeta) = \frac{1}{(\zeta - i\chi)^2}$ we find from the series (2.23) that

$$f_{-k} = \frac{1}{2\pi} \int_{-\infty}^{\infty} \frac{1}{(\zeta - i\chi)^2} \left(\frac{\zeta - i}{\zeta + i} \right)^k (-1)^k \frac{2}{\zeta^2 + 1} d\zeta, \quad k \geq 0. \quad (2.29)$$

Closing the complex integration contour in the upper half-plane of ζ one obtains from equation (2.29) that

$$f_{-k} = i \frac{d}{d\zeta} \left(\frac{\zeta - i}{\zeta + i} \right)^k (-1)^k \frac{2}{\zeta^2 + 1} \theta(\chi) \Big|_{\zeta=i\chi} + \delta_{k,0} \frac{1}{(i - i\chi)^2}, \quad k \geq 0 \quad (2.30)$$

and

$$f_0 = -\frac{1}{[1 + \chi \operatorname{sign}(\chi)]^2}. \quad (2.31)$$

Taking a sum over k in equation (2.24), using equations (2.30) and (2.31) and we find that

$$\hat{P} \frac{1}{(\zeta - i\chi)^2} = \frac{1}{(\zeta - i\chi)^2} \theta(\chi) + \frac{1}{(i - i\chi)^2} \theta(-\chi) + \frac{1}{2[1 + \chi \operatorname{sign}(\chi)]^2}. \quad (2.32)$$

2.2. Integral representation of the equation for Stokes wave

Using equations (2.20), (2.28) and (2.32) we obtain the following projections in terms of $\rho(\chi)$:

$$\hat{P} f = \int_{\chi_c}^1 \frac{\rho(\chi) d\chi}{\zeta - i\chi} - \int_{\chi_c}^1 \frac{i\rho(\chi) d\chi}{2(1 + \chi)}, \quad \hat{P} \bar{f} = - \int_{\chi_c}^1 \frac{i\rho(\chi) d\chi}{2(1 + \chi)}. \quad (2.33)$$

We now find $\hat{P} [\bar{f} f_u]$ used in (2.22). Equation (1.6) results in the following expression

$$\bar{f} f_u = \frac{\zeta^2 + 1}{2} \bar{f} f_\zeta = -\frac{\zeta^2 + 1}{2} \int_{\chi_c}^1 \int_{\chi_c}^1 \frac{\rho(\chi') \rho(\chi'') d\chi' d\chi''}{(\zeta + i\chi')(\zeta - i\chi'')^2}. \quad (2.34)$$

We perform the partial fraction decomposition of the integrand of (2.34) as follows

$$-\frac{\zeta^2 + 1}{2(\zeta + i\chi')(\zeta - i\chi'')^2} = \frac{1}{\zeta + i\chi'} \frac{1 - \chi'^2}{2(\chi' + \chi'')^2} + \frac{1}{\zeta - i\chi''} \frac{-1 - 2\chi'\chi'' - \chi''^2}{2(\chi' + \chi'')^2} + \frac{1}{(\zeta - i\chi'')^2} \frac{i(1 - \chi''^2)}{2(\chi' + \chi'')}. \quad (2.35)$$

and apply the projector \hat{P} to (2.35) which gives with the use of (2.28) and (2.32) the following expression:

$$\begin{aligned} \hat{P} [\bar{f} f_u] = & \int_{\chi_c}^1 \int_{\chi_c}^1 \left[\frac{1}{i + i\chi'} \frac{1 - \chi'^2}{4(\chi' + \chi'')^2} + \left(\frac{1}{\zeta - i\chi''} - \frac{i}{2(1 + \chi'')} \right) \frac{-1 - 2\chi'\chi'' - \chi''^2}{2(\chi' + \chi'')^2} \right. \\ & \left. + \left(\frac{1}{(\zeta - i\chi'')^2} + \frac{1}{2(1 + \chi'')^2} \right) \frac{i(1 - \chi''^2)}{2(\chi' + \chi'')} \right] \rho(\chi') \rho(\chi'') d\chi' d\chi''. \end{aligned} \quad (2.36)$$

The other nonlinear term in equation (2.22) has the following integral form

$$ff_u = \frac{1}{2}(1 + \zeta^2)ff_\zeta = -\frac{1}{2}(1 + \zeta^2) \int_{\chi_c}^1 \frac{\rho(\chi')d\chi'}{(\zeta - i\chi')} \int_{\chi_c}^1 \frac{\rho(\chi'')d\chi''}{(\zeta - i\chi'')^2}. \quad (2.37)$$

The constant y_b is determined from equation (2.15) as follows

$$\int_{-\pi}^{\pi} y(1 + \tilde{x}_u)du = \int_{-\infty}^{\infty} \left[y_b + \frac{(f - \bar{f})}{2i} \right] \left[1 + \frac{(1 + \zeta^2)}{4}(f_\zeta + \bar{f}_\zeta) \right] \frac{2d\zeta}{1 + \zeta^2} = 0, \quad (2.38)$$

which results using equation (2.20) in the following equation

$$y_b = - \int_{\chi_c}^1 \int_{\chi_c}^1 \frac{\rho(\chi')\rho(\chi'')d\chi'd\chi''}{2(\chi' + \chi'')^2} - \int_{\chi_c}^1 \frac{\rho(\chi')d\chi'}{1 + \chi'}. \quad (2.39)$$

Equation (2.39) allows to find y_b from a given $\rho(\chi)$. This equation also provides a convenient tool to estimate the accuracy of recovering $\rho(\chi)$ by Padé approximation. For that one compares the numerical value of y_b obtained from the Stokes solution in Part I (Dyachenko *et al.* 2016) with the result of the direct numerical calculation of right-hand side (r.h.s.) of equation (2.39) with $\rho(\chi)$ obtained from Padé approximation in Part I (all these numerical values are given in tables of Part I (Dyachenko *et al.* 2016), through the electronic attachment to Ref. Dyachenko *et al.* (2015a) and at the web link Dyachenko *et al.* (2015b)).

Integrating equation (2.20) in u over 2π -period one obtains the zero Fourier harmonic y_0 of $y(u)$ as follows

$$y_0 = y_b + \int_{\chi_c}^1 \frac{\rho(\chi')d\chi'}{1 + \chi'}. \quad (2.40)$$

Requiring that equations (2.20)-(2.22), (2.33), (2.36), (2.37) and (2.39) are satisfied for $-\infty < \zeta < \infty$ we obtain a system of equations to find the density $\rho(\chi)$ along the branch cut for each c . That system has a form of nonlinear integral equation for the unknown function $\rho(\chi)$. Taking the limit $\zeta \rightarrow \infty$ in that system results in the following compact expression

$$\begin{aligned} & \frac{c^2}{2} \int_{\chi_c}^1 \rho(\chi')d\chi' + 2 \left[- \int_{\chi_c}^1 \int_{\chi_c}^1 \frac{\rho(\chi')\rho(\chi'')d\chi'd\chi''}{2(\chi' + \chi'')^2} - \int_{\chi_c}^1 \frac{\rho(\chi')d\chi'}{1 + \chi'} \right] \\ & \times \left[1 - \frac{1}{2} \int_{\chi_c}^1 \rho(\chi''')d\chi''' \right] + \int_{\chi_c}^1 \frac{\rho(\chi')d\chi'}{1 + \chi'} + \int_{\chi_c}^1 \int_{\chi_c}^1 \frac{(1 - \chi')\rho(\chi')\rho(\chi'')d\chi'd\chi''}{2(\chi' + \chi'')^2} = 0, \end{aligned} \quad (2.41)$$

which can be used to find c from the given $\rho(\chi)$.

2.3. Numerical solution for Stokes wave based on the integral representation

To solve the system (2.20)-(2.22), (2.33), (2.36), (2.37) and (2.39) numerically we use the approximation of the integral in equation (2.18) by the following numerical quadrature

$$f(u) = \tilde{z}(\zeta) - iy_b = \int_{\chi_c}^1 \frac{\rho(\chi')d\chi'}{\zeta - i\chi'} \simeq \sum_{j=1}^N \frac{\gamma_j}{\zeta - i\chi_j}, \quad (2.42)$$

which has a form of Padé approximation at the discrete set of points $\chi_c < \chi_1 < \chi_2 < \dots < \chi_N < 1$ with weights γ_j , $j = 1, 2, \dots, N$. Then the analysis of Sections 2.1 and 2.2 with equation (2.18) replaced by the approximation (2.42) is carried out in exactly the same way as in equations (2.20)-(2.39) with each time $\rho(\chi)d\chi$ and χ replaced by γ_j and χ_j , respectively. Also integrals are replaced by the summations. It results in the discrete versions of these equations including

$$\hat{P}f = \sum_{j=1}^N \frac{\gamma_j}{\zeta - i\chi} - \sum_{j=1}^N \frac{i\gamma_j}{2(1 + \chi)}, \quad \hat{P}\bar{f} = - \sum_{j=1}^N \frac{i\gamma_j}{2(1 + \chi)}, \quad (2.43)$$

$$ff_u = -\frac{1}{2}(1 + \zeta^2) \sum_{j'=1}^N \frac{\gamma_{j'}}{(\zeta - i\chi_{j'})} \sum_{j''=1}^N \frac{\gamma_{j''}}{(\zeta - i\chi_{j''})^2} \quad (2.44)$$

and

$$\begin{aligned} \hat{P}[\bar{f}f_u] &= \sum_{j'=1}^N \sum_{j''=1}^N \left[\frac{1}{i + i\chi_{j'}} \frac{1 - \chi_{j''}^2}{4(\chi_{j'} + \chi_{j''})^2} + \left(\frac{1}{\zeta - i\chi_{j''}} - \frac{i}{2(1 + \chi_{j''})} \right) \right. \\ &\times \left. \frac{-1 - 2\chi_{j'}\chi_{j''} - \chi_{j''}^2}{2(\chi_{j'} + \chi_{j''})^2} + \left(\frac{1}{(\zeta - i\chi_{j''})^2} + \frac{1}{2(1 + \chi_{j''})^2} \right) \frac{i(1 - \chi_{j''}^2)}{2(\chi_{j'} + \chi_{j''})} \right] \gamma_{j'}\gamma_{j''}. \end{aligned} \quad (2.45)$$

Also equation (2.39) is replaced in the same discrete approximation by the following equation

$$y_b = - \sum_{j'=1}^N \sum_{j''=1}^N \frac{\gamma_{j'}\gamma_{j''}}{2(\chi_{j'} + \chi_{j''})^2} - \sum_{j'=1}^N \frac{\gamma_{j'}}{1 + \chi_{j'}}. \quad (2.46)$$

Choosing numerical values γ_j , χ_j , $j = 1, 2, \dots, N$ from Padé approximants of Part I (Dyachenko *et al.* 2016) (these approximants are also available through the electronic attachment to Ref. Dyachenko *et al.* (2015a) and at the web link Dyachenko *et al.* (2015b)) we checked that equation (2.22) (together with equations (2.43)-(2.46)) is valid for each value of H/λ with the same numerical precision as the precision (at least 10^{-26}) of the Stokes solutions of Part I (Dyachenko *et al.* 2016). Values of N in Part I range between tenths for moderate values of H/λ up to $N = 92$ for the highest Stokes wave considered (given by Table 4 in Part I (Dyachenko *et al.* 2016)). These moderate numbers is in sharp contrast with the large number M of Fourier modes required for constructing these solutions with the same precision ($M \simeq 1.3 \cdot 10^8$ for the highest Stokes wave considered in Table 4 of Part I). An explanation for that dramatic difference between required numerical values of M and N follows from Part I. It was found in Part I that the error of Fourier method scales as $\propto \exp(-2\chi_c M)$ while the error for Padé approximation of Part I is $\propto \exp(-c_1 \chi_c^{1/6} M)$, $c_1 \sim 1$. It suggests that solving equations (2.22), (2.43)-(2.46) for numerical values of γ_j , χ_j , $j = 1, 2, \dots, N$ is the attractive alternative to the numerical methods of Part I.

To solve equations (2.22), (2.43)-(2.46) numerically, we aim to approximately satisfy equation (2.22) at the discrete set of points $-\infty < \zeta = \zeta_i < \infty$, $i = 1, 2, \dots, M_1$. It results in the nonlinear algebraic system of equations to find γ_j , χ_j , $j = 1, 2, \dots, N$. That system is overdetermined (see e.g. Ref. Wilkening & Yu (2012) as the example of using of overdetermined systems for simulating water waves) provided we choose $M_1 > 2N$ but it can be solved in least square sense (by minimizing the sum of squares of the left-hand side (l.h.s.) of equation (2.22) taken over points $\zeta = \zeta_i$, $i = 1, 2, \dots, M_1$). However,

the difficulty in such most straightforward approach is in extreme ill-conditioning of the resulting algebraic system mainly because of denominators containing large powers of χ_j clearly seen if we try to bring equation (2.22) to the common denominator. We bypass that difficulty here by providing the explicit procedure to find the appropriate values of χ_j , $j = 1, 2, \dots, N$ for each χ_c (see the description of that procedure below in this Section) and only after that we solve equations (2.22), (2.43)-(2.46) for unknowns γ_j , $j = 1, 2, \dots, N$ at the discrete set of points $-\infty < \zeta = \zeta_i < \infty$, $i = 1, 2, \dots, M_1$. Then the resulting system is the cubic polynomial in γ_j , $j = 1, 2, \dots, N$. That system is still moderately ill-conditioned but that difficulty is easily overcome by choosing M_1 large enough with Newton's iterations used to find numerical values of γ_j , $j = 1, 2, \dots, N$, thus forming least-square-Newton (LSN) algorithm. E.g., for $H/\lambda = 0.1387112446\dots$ (corresponds to $\chi_c = 3.0056373876\dots \cdot 10^{-3}$, see also table 1 of Appendix C for details on numerical Stokes waves) we found that it is sufficient to use $M_1 = 800$ and $N = 51$ to achieve 10^{-19} accuracy for Stokes wave. For steeper Stokes waves with $H/\lambda = 0.1401109676\dots$ ($\chi_c = 6.99513864872\dots \cdot 10^{-4}$) and $H/\lambda = 0.1408682599\dots$ ($\chi_c = 5.6590609636\dots \cdot 10^{-5}$) we found that using $M_1 = 1600$, $N = 61$ and $M_1 = 10^4$, $N = 78$ allow to achieve 10^{-18} and 10^{-19} accuracy, respectively. Here values of N were chosen the same as for the respective Stokes wave in Part I while M_1 is by a factor ~ 80 smaller than $M = 65536$ in the first case and by a factor ~ 200 smaller than $M = 2097152$ in the third case (values of M are given in Part I, through the electronic attachment to Ref. Dyachenko *et al.* (2015a) and at the web link Dyachenko *et al.* (2015b)). In these examples, using the symmetry of Stokes wave, the points ζ_j were chosen to have nonnegative values with the first 300 points uniformly spaced as $\zeta_i = (i-1)2\pi/M$, $i = 1, \dots, 300$ and the remaining $M_1 - 300$ points uniformly (in u) spanning the remaining interval of positive values of ζ . After values of γ_j , $j = 1, 2, \dots, N$ are found from LSN algorithm, equation (2.42) provides Padé approximation for Stokes wave at the entire real line of ζ . Then one can use the results of Section 6.1 to find the high precision numerical approximation of χ_c , which completes the current step in H/λ (or equivalently the current step in χ_c). These step are repeated to gradually increase H/λ (or equivalently decrease χ_c) by changing the velocity parameter c to span the desired range of Stokes waves.

The procedure to find the grid χ_j , $j = 1, 2, \dots, N$ at each step is the following. Assume that $\chi_c < \chi_1 < \chi_2 < \dots < \chi_{N-1} < \chi_N < 1$ and $\chi_c \ll 1$. We use the property of Stokes wave that $\rho(\chi)$ changes a little vs. a change of H/λ for $\chi \gg \chi_c$ provided $\chi_c \ll 1$. It implies that χ_j can be chosen independently on χ_c for all j such that $\chi_j \gg \chi_c$. In numerical examples above we chose numerical values in the range $\chi_j \gg \chi_c$ from Padé data for Stokes wave with $H/\lambda = 0.1409700957\dots$ obtained in Part I (Dyachenko *et al.* 2016). Also the grid χ_j can be chosen from the grid obtained at the previous step (with a previous smaller value of χ_c).

We now consider the construction of grid for smaller values of χ_j . If we assume a power law singularity $\rho(\chi) \propto (\chi - \chi_c)^\alpha$, $\alpha > 0$ and consider the limit $\zeta \rightarrow i\chi_c$ in equation (2.18), then the transformation to a new integration variable $t = (\chi - \chi_c)^\alpha$ removes the singularity from the integrand in equation (2.18). The uniform grid $t_j = j\Delta t$, $j = 1, 2, \dots$, $\Delta t = \text{const}$ in t is the natural choice to use for the integration in the variable t . The corresponding grid in χ is given by

$$\chi_j - \chi_c = t_j^{1/\alpha} = j^{1/\alpha} \Delta t^{1/\alpha}. \quad (2.47)$$

Stokes wave has the square root singularity at $\zeta = i\chi_c$ with the expansion

$$\tilde{z}(\zeta) - iy_b = f(\zeta) = \sum_{j=0}^{\infty} i e^{i j \pi / 4} a_j (\zeta - i\chi_c)^{j/2}, \quad (2.48)$$

where a_j are real constants (see Part I (Dyachenko *et al.* 2016) as well as Sections 6 and 7 below for the justification of that expansion). It implies (see Part I) the square root singularity for the density $\rho(\chi) \propto (\chi - \chi_c)^{1/2}$ in the integrand of equation (2.18). Using equation (2.47) with $\alpha = 1/2$ one then obtains that

$$\chi_j - \chi_c = \Delta t^2 j^2, \quad j \sim 1, \quad (2.49)$$

which is in the excellent agreement with numerical values of χ_j obtained in Part I provided $\Delta t^2 \sim 0.01\chi_c$.

In the range $\chi_c \ll \chi \ll 1$, the density $\rho(\chi) \propto \chi^{2/3}$ is well approximated by the density $\rho(\chi) \propto \chi^{2/3}$ of the limiting Stokes wave (1.1) as shown in Figure 8 of Part I. Using equation (2.47) with $\alpha = 2/3$, one obtains that

$$\chi_j = c j^{3/2}, \quad (2.50)$$

where c is the positive constant and $j \gg 1$ such that $\chi_j \ll 1$. We additionally have to approximate the transition between two scalings (2.49) and (2.50) at the intermediate values of j . Exploring fits of χ_j vs. j for multiple sets of numerical data of Part I we found that a satisfactory fit (including the required transition) is given by the linear combination of the scaling (2.49) and (2.50) superimposed with the exponential growth in j as follows

$$\chi_j = \chi_c \left[c_1 j^2 + c_2 j^{3/2} e^{c_3 j} \right], \quad (2.51)$$

where the positive fitting constant c_1 , c_2 and c_3 changes slowly with χ_c (change of χ_c in 5 orders of magnitude results in change of these constants by less than 50%).

Based on these observations we implemented the following procedure to find numerical values of c_1 , c_2 and c_3 for each value of χ_c . We choose N from the previous step (with the previous value of χ_c). (If performing the current step we are not able to reach the desired precision with the increase of M_1 , i.e. LSN algorithm would not converge to the prescribed tolerance, e.g. 10^{-16} , then N has to be increased by 1 and the current step restarted from the beginning). Next we choose j_{match} from the values χ_j of Table 4 of Part I (or from the grid obtained at the previous step in χ_c) such that $\chi_{j_{match}}/\chi_c \sim 100$ which well ensures the required condition $\chi_j \gg \chi_c$. (For larger values of χ_c one can use a smaller value of $\chi_{j_{match}}/\chi_c$ to make sure that $\chi_{j_{match}} \ll 1$. E.g. for the case $H/\lambda = 0.1387112446\dots$ (first numerical case mentioned above in this section) we choose $\chi_{j_{match}}/\chi_c \sim 34$.) After choosing the value of j_{match} , we perform 4th order interpolation of χ_j as the function of j and find values of the first and second derivatives, χ'_j and χ''_j , of that interpolant at $j = j_{match}$. We use these 3 numerical values $\chi_{j_{match}}$, $\chi'_{j_{match}}$ and $\chi''_{j_{match}}$ to find the numerical values of c_1 , c_2 and c_3 by matching the corresponding values of equation (2.51) and its two derivatives at $j = j_{match}$. Then equation (2.51) provides the numerical values of χ_j , $j = 1, 2, \dots, j_{match}$ completing the construction of the numerical grid χ_j , $j = 1, 2, \dots, N$ for the current step in χ_c . (If any of the constants c_1 , c_2 or c_3 turns negative then one has to decrease $\chi_{j_{match}}/\chi_c$ to avoid that but in our numerical examples we experienced such problems only if $\chi_{j_{match}}/\chi_c$ was chosen $\gtrsim 10^3$). Then LSN algorithm is used as described above.

The efficiency of the grid χ_j , $j = 1, 2, \dots, N$ thus obtained requires a good initial estimate of χ_c with the relative accuracy $\sim 10^{-3}$. It is achieved by a gradual increase

of H/λ (decrease of χ_c) at multiple previous steps of LSN algorithm. Values of χ_c are found at each previous step with high precision by the procedure of Section 6.1. The polynomial extrapolation of χ_c to the current step is performed to reach the needed relative accuracy $\sim 10^{-3}$. Note that the numerical detection of the incorrect value of χ_c prediction is straightforward because it would cause the oscillations of γ_j (with changing of its sign) around several smallest values of the index $j = 1, 2, 3, \dots$

We would like to stress the difference of LSN algorithm of this Section compare with the method of Part I (Dyachenko *et al.* 2016). Stokes wave was obtained in Part I by using the Fourier series representation of the solution combined with Newton-Conjugate-Gradient iterations method. After that the resulting solution was approximated at the real line of ζ by a numerically stable version of the Padé algorithm. Thus Padé approximants of Part I were only the auxiliary tool to compactly represent the result of calculation of Stokes waves. In contrast, in this Section we completely bypass the Fourier series representation and numerically solve integral equations (2.22), (2.43)-(2.46) directly by Padé approximants. The cost of the approach of this Section is that instead of $2N$ free parameters χ_j, γ_j , $N = 1, 2, \dots, N$ of Padé approximants of Part I, we now have only N free parameters γ_j , $N = 1, 2, \dots, N$, while the values of χ_j , $N = 1, 2, \dots, N$ are fixed by the grid algorithm described previously in this section. It means that to achieve the same precision we need to approximately double the value of N compare with Part I. This is however very moderate cost compare with the Fourier method of Part I.

In conclusion, in this Section we demonstrated the performance LSN algorithm for several values of χ_c which were previously explored in Part I by the Fourier method. We expect that much smaller values of N , required for LSN algorithm compare with Fourier method, will allow to find Stokes waves for much smaller values of χ_c than achievable by Fourier method of Part I. In addition, equation (2.41) can be used to exclude c from the system allowing to gradually increase H/λ (or equivalently decrease χ_c) thus avoiding the problem of nonmonotonic dependence of c on H/λ encountered in Part I. The detailed practical realization of that limit of smaller χ_c is beyond the scope of this paper.

3. Alternative form for the equation of Stokes wave

The equation for Stokes wave can be written in a form which is alternative to equation (2.1) as follows

$$y = -\frac{i}{2}(\tilde{z} - \bar{\tilde{z}}) = -\frac{i}{2}(z - \bar{z}) = \frac{c^2}{2} \left(1 - \frac{1}{|z_u|^2} \right). \quad (3.1)$$

Appendix A shows the equivalence of both forms of equations (2.1) and (3.1) for Stokes wave. Also Appendix B discusses differences in derivation of equations (2.1) and (3.1) from basic equations of the potential flow of ideal fluid with free surface. Different versions of equation (3.1) (up to trivial scaling of parameters and shift of y by different constants) were used by Grant (1973), Williams (1981), Plotnikov (1982) and Tanveer (1991).

Transforming equation (3.1) into the variable ζ (1.6) results in

$$\tilde{z} - \bar{\tilde{z}} = ic^2 \left(1 - \frac{4}{(1 + \zeta^2)^2 |z_\zeta|^2} \right). \quad (3.2)$$

Solving equation (3.1) for z_u , one obtains that

$$z_u = \frac{c^2}{\bar{z}_u [i(z - \bar{z}) + c^2]} \quad (3.3)$$

which is the nonlinear ODE provided \bar{z}_u is known. In a similar way, equation (3.2) results

in

$$z_\zeta = \frac{4}{(1 + \zeta^2)^2} \frac{c^2}{\bar{z}_\zeta [i(z - \bar{z}) + c^2]}. \quad (3.4)$$

Equations (3.3) and (3.4) can be considered as ODEs for $z(u)$ and $z(\zeta)$, respectively, if \bar{z} is the known function. Then solving ODE provides a convenient tool to study the analytical properties of Stokes wave in different sheets of Riemann surface of z .

4. Asymptotic of Stokes wave at $Im(w) \rightarrow +\infty$ and jump at branch cut

An asymptotical solution of Stokes wave in the limit $Im(w) \rightarrow +\infty$ is obtained from equation (3.3) as follows. Equation (2.9) implies the exponential convergence $\propto e^{-iw}$ of $\tilde{z}(w)$ to its zeroth Fourier harmonic, $\tilde{z}(w) \rightarrow iy_0$ for $Im(w) \rightarrow -\infty$. Here y_0 is determined by the mean-zero elevation condition (2.15) and is given by equations (2.39) and (2.40). Respectively, $\bar{\tilde{z}}(w)$ converges exponentially to $-iy_0$ for $Im(w) \rightarrow \infty$. Then \bar{z}_u and \bar{z} in equation (3.3) can be replaced by 1 and $-iy_0$, respectively in that limit resulting in

$$1 + \tilde{z}_u = \frac{c^2}{i(\tilde{z} + iy_0) + c^2}, \quad Im(w) \rightarrow \infty. \quad (4.1)$$

Integrating equation (4.1) in the upper right quadrant $w \in \mathbb{C}^+$, $Re(w) > 0$ for $v \gg 1$, one obtains that

$$\tilde{z}(w) - ic^2 \ln [\tilde{z}(w) + iy_0] = -w + c_+, \quad (4.2)$$

where c_+ is the constant. A similar integration in the upper left quadrant $w \in \mathbb{C}^+$, $Re(w) < 0$, for $v \gg 1$ results in

$$\tilde{z}(w) - ic^2 \ln [\tilde{z}(w) + iy_0] = -w + c_-, \quad (4.3)$$

where c_- is the constant.

Taking $w = \pi + iv$ in equation (4.2) and $w = -\pi + iv$ in equation (4.3) together with the periodicity condition $\tilde{z}(\pi + iv) = \tilde{z}(-\pi + iv)$ result in the condition for constants c_+ and c_- as follows

$$c_- - c_+ = -2\pi. \quad (4.4)$$

Exponents of equations (4.2) and (4.3) are similar to the Lambert W -function. Solving these equations in the limit $v \rightarrow \infty$ (see e.g. Refs. Dyachenko *et al.* (2013b); Lushnikov *et al.* (2013) for details on a similar technique) one obtains that

$$\begin{aligned} \tilde{z}(w) = -w + c_\pm + ic^2 \ln [-w + c_\pm + iy_0] - \frac{c^4 \ln [-w + c_\pm + iy_0]}{-w + c_\pm + iy_0} \\ + O\left(\frac{\ln [-w + c_\pm + iy_0]}{-w + c_\pm + iy_0}\right)^2, \end{aligned} \quad (4.5)$$

where a use of c_+ and c_- assumes that $Re(w) > 0$ and $Re(w) < 0$, respectively. If equation (3.3) is used instead of the reduced equation (4.1) in derivation of equation (4.5), then an additional exponentially small error term $O(e^{-v}/v)$ appears in r.h.s. of equation (4.5). The two leading order terms $-w + c_\pm$ and $ic^2 \ln [-w + c_\pm + iy_0]$ in r.h.s. of equation (4.5) are similar to equation (2.22) of Ref. Tanveer (1991), where these terms were derived in somewhat similar procedure to the derivation of equation (4.5).

One concludes from equation (4.5) that $z(w)$ has a complex singularity at $z = \infty$ which involves logarithms with the infinite number of sheets of Riemann surface. Full analysis of that singularity requires to study next order terms in equation (4.5) which is beyond the scope of this paper.

Taking an additional limit $w = iv \pm \epsilon$, $\epsilon > 0$, $\epsilon \rightarrow 0$ in equation (4.1), using the condition (4.4) and expanding in $v \gg 1$, one obtains the jump at the branch cut

$$z(iv - 0) - z(iv + 0) = -2\pi + \frac{2\pi c^2}{v} + O(v^{-2}), \quad (4.6)$$

where the branch cut $v \in [iv_c, i\infty]$ is crossed in counterclockwise direction.

According to equation (2.19), the jump (4.6) is related to the density $\rho(\chi)$ (2.18) as follows

$$\rho(\chi)|_{\chi=\tanh(v/2)} = 1 - \frac{c^2}{v} + O(v^{-2}), \quad v \gg 1. \quad (4.7)$$

For $v \gg 1$, one obtains from equation (1.6) that $1 - \chi \ll 1$ and $v = -\ln\left(\frac{1-\chi}{2}\right) + O(1 - \chi)$. Then the density (4.7) takes the following form

$$\rho(\chi) = 1 + \frac{c^2}{\ln\left(\frac{1-\chi}{2}\right)} + O\left(\frac{1}{\ln^2(1-\chi)}\right). \quad (4.8)$$

Equation (4.8) implies a unit value

$$\rho(1) = 1 \quad (4.9)$$

and the divergence of the derivative

$$\frac{d\rho(\chi)}{d\chi} \simeq \frac{c^2}{(1-\chi)\ln^2\left(\frac{1-\chi}{2}\right)} \rightarrow \infty \text{ for } \chi \rightarrow 1. \quad (4.10)$$

5. Numerical procedure to analyze the structure of sheets of Riemann surface for Stokes wave by ODE integration

We use Padé approximants of Stokes wave found in Part I (Dyachenko *et al.* 2016) and provided both in tables of Part I, through the electronic attachment to Ref. Dyachenko *et al.* (2015a) and at the web link Dyachenko *et al.* (2015b) in the following form

$$z_{pade}(u) \equiv u + iy_b + \sum_{n=1}^N \frac{\gamma_n}{\tan(u/2) - i\chi_n}, \quad (5.1)$$

with the numerical values of y_b , the pole positions χ_n and the complex residues γ_n ($n = 1, \dots, N$) given there. These data of Padé approximation allow to recover the Stokes wave at the real axis $w = u$ (and similar at $\zeta = Re(\zeta)$ in the complex ζ -plane) with the relative accuracy of at least 10^{-26} (for the vast majority of numerical cases the actual accuracy is even higher by several orders of magnitude).

Analytical continuation of the Padé approximant (5.1) from u to $w \in \mathbb{C}$ is given by the straightforward replacing of u by w . That analytical continuation is accurate for $w \in \mathbb{C}^-$ but loses precision for $w \in \mathbb{C}^+$ in the neighbourhood of the branch cut $w \in [iv_c, i\infty)$ where the discrete sum (5.1) fails to approximate the continuous parameterization (2.18) of the branch cut. Thus a significant loss of precision compare to 10^{-26} occurs only if the distance from the given value of ζ to the branch cut is smaller or comparable with the distance between neighbouring values of χ_n in equation (5.1).

Numerical integrations of ODE (3.4) (and occasionally ODE (3.3)) in this Section were performed using 9(8)th order explicit Runge-Kutta algorithm with adaptive stepping embedded into Mathematica 10.2 software. That algorithm is the implementation of Ref. Verner (2010) and is based on the embedded pair of 9th and 8th order methods with higher order method used for the adaptive step-size control. We used the numerical

precision of 55 digits and reached the accuracy 10^{-30} to make sure that no significant accumulation of ODE integration error occurs in comparison with 10^{-26} precision of the Padé approximants of Stokes waves. We also independently verified the accuracy of the numerical ODE integration by comparing with the analytical results of Section 6 in the neighborhoods of $\zeta = \pm i\chi_c$ in multiple sheets of Riemann surface.

At the first step of our investigation, ODE (3.4) was solved numerically to find the approximation $z_{ODE}(\zeta)$ for $z(\zeta)$ with $\zeta \in \mathbb{C}^+$ in the first and the second sheet of Riemann surface using the approximants (5.1) for \bar{z} and \bar{z}_ζ . Here the first (physical) sheet of Riemann surface corresponds to $z(\zeta)$ with fluid occupying $\zeta \in \mathbb{C}^-$. The second (non-physical) sheet is reached when the branch cut $\zeta \in [i\chi_c, i]$ (or equivalently $w \in [iv_c, i\infty)$) is crossed from the first sheet. That ODE was solved with initial conditions at real line $\zeta = Re(\zeta)$ by integrating along different contours in $\zeta \in \mathbb{C}^+$. A high precision of at least 10^{-30} was achieved in ODE solver to avoid any significant additional loss of precision compare with 10^{-26} precision of equation (5.1). That ODE solution used \bar{z}_{pade} and $(\bar{z}_{pade})_\zeta$ which through the complex conjugation corresponds to the approximants (5.1) in $\zeta \in \mathbb{C}^-$ thus avoiding any loss of precision compare with 10^{-26} . We stress here that the use of Padé approximation is the auxiliary tool which does not make any difference in the final result because it matches the precision of Fourier series. The Fourier series of Part I can be used directly instead of Padé approximants which however would require significant increase of computational resources to reach the same precision.

The left panel of Figure 2 shows a typical $0BCDA0$ rectangular contour for ODE integration which was used for the analytical continuation of Stokes wave into the second sheet of Riemann surface. The ODE solution in the second sheet is obtained when integrating contour crosses the branch cut $[i\chi_c, i]$. The second subsequent crossing of that branch cut returns $z_{ODE}(\zeta)$ to the first sheet confirming the square root branch point at $\zeta = i\chi_c$. Figure 3 provides a numerical example of such double crossing. In other words, it was found that ODE integration along any closed contour in $\zeta \in \mathbb{C}^+$ with double crossing of the branch cut (twice integrating along $0BCDA0$) always returns the solution to the original one. If the height of $0BCDA0$ contour is made smaller than χ_c then there is no crossing of the branch cut and $0BCDA0$ integration returns to the initial value after a single round trip as shown by dashed curves of Figure 3. In similar way, if the height of $0BCDA0$ exceeds 1 then there is no crossing and $z_{ODE}(\zeta)$ stays in the first sheet (crossing of the branch cut $(i, i\infty)$ corresponds to the jump on 2π in u direction in w plane while there is no jump in \bar{z} because of 2π -periodicity).

We also verified that there are no singularities in the limit $|Re(\zeta)| \rightarrow \infty$ by switching to ODE integration (3.3) in w variable. In that limit $Re(w) \rightarrow \pm\pi$ which allows to extend the contour in w over the entire 2π period in u direction (in ζ variable it would require to integrate over the infinite interval $-\infty < Re(\zeta) < \infty$). For all subsequent cases in this section it is assumed that such integration in w was performed to check the limit $Re(w) \rightarrow \pm\pi$.

The second step of our investigation was to find $z(\zeta)$ by integrating ODE (3.4) in the second sheet with $\zeta \in \mathbb{C}^-$ using the complex conjugate of $z_{ODE}(\zeta)$, $\zeta \in \mathbb{C}^+$ found at previous step to approximate \bar{z} and \bar{z}_ζ . Initial condition at that step was at the real line $\zeta = Re(\zeta)$ with $z(\zeta)$ obtained at the step one for the second sheet.

The second step reveals a new square root singularity at $\zeta = -i\chi_c$ in the second sheet. Similar to the step one, the double integration over the contour $ABEFA$ shows that $z(\zeta)$ returns to its original value confirming that $\zeta = -i\chi_c$ is the square root branch point. Crossing of the branch cut $[-i\chi_c, -i]$ (corresponds to that new branch point $\zeta = -i\chi_c$) allows to go into the third sheet of Riemann surface. At that crossing one has to simultaneously cross from the first to the second sheets for \bar{z} and \bar{z}_ζ which again are the

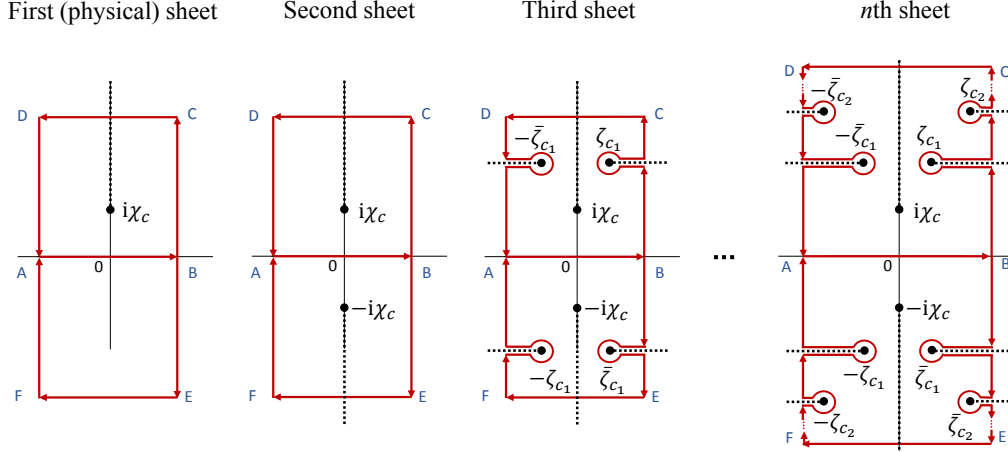


FIGURE 2. A schematic of integrating contours in different sheets of Riemann surface in the complex variable ζ (1.6) near the origin. The first (physical) sheet has a square root singularity only at $\zeta = i\chi_c$ in \mathbb{C}^+ . Then integrating ODE (3.4) over the closed contour $ABCD A$ provides the analytical continuation into the second sheet of Riemann surface as the branch cut (dashed line) is crossed. As a result, $z(\zeta)$ does not return to its initial value at the origin 0. In contrast, integrating ODE (3.4) over the closed contour $ABEFA$ (or over $ABCD A$ provided its height falls below $\zeta = i\chi_c$), one does not cross the branch cut so $z(\zeta)$ returns to the same value at the origin with $z(\zeta)$ remaining in the first sheet. The second sheet has the second square root branch point singularity at $\zeta = -i\chi_c$ at the lower complex half-plane \mathbb{C}^- . Integrating over contour $ABEFA$ in the second sheet results in the analytical continuation of $z(\zeta)$ into the third sheet of Riemann surface. Starting from the third sheet, extra square root branch points appear away from the imaginary axis. Branch cuts for these off-axis singularities are chosen to be extended horizontally as shown by dashed lines in the two right panels. The number of these branch points grows with the growth of the sheet number as schematically shown in the right panel. We avoid crossing these branch by modifying contours $ABCD A$ and $ABEFA$ as shown in the two right panels. Note that these two contours must be symmetric with respect to the real line even if the chosen pair of off-axis singularities (symmetric with respect to the imaginary axis) are located only in one of the complex half-planes \mathbb{C}^+ and \mathbb{C}^- in the given sheet. This is because $\bar{z}(\zeta)$ is needed for the integration of ODE (3.4).

complex conjugate of $z_{ODE}(\zeta)$, $\zeta \in \mathbb{C}^+$ found at previous step. It was found that the third sheet has branch points both at $\zeta = i\chi_c$ and $\zeta = -i\chi_c$. In a similar way to previous steps, at the step three one crosses the branch cut $[i\chi_c, i]$ to go into the fourth sheet of Riemann surface which found to has branch points both at $\zeta = i\chi_c$ and $\zeta = -i\chi_c$. At the step four one crosses the branch cut $[-i\chi_c, -i]$ to go into the fifth sheet of Riemann surface which again has branch points both at $\zeta = i\chi_c$ and $\zeta = -i\chi_c$ etc. At each sheet, \bar{z}, \bar{z}_ζ used in integration of ODE (3.4) is behind by one in sheet number to the current sheet, i.e. values of \bar{z}, \bar{z}_ζ from the first, second, third etc. sheets are used for ODE integration in the second, third, fourth etc. sheets, respectively. After exploring several hundreds of sheets for different values of χ_c , one concludes that the number of sheets is infinite. The double integration over the contours $ABCD A$ and $ABEFA$ shows that $\zeta = i\chi_c$ and $\zeta = -i\chi_c$ are square root branch points in all sheets. In the next section this conjecture is strengthened by the analysis of expansions at $\zeta = \pm i\chi_c$ in these multiple sheets.

Starting from the third sheet, extra square root branch points appear away from the

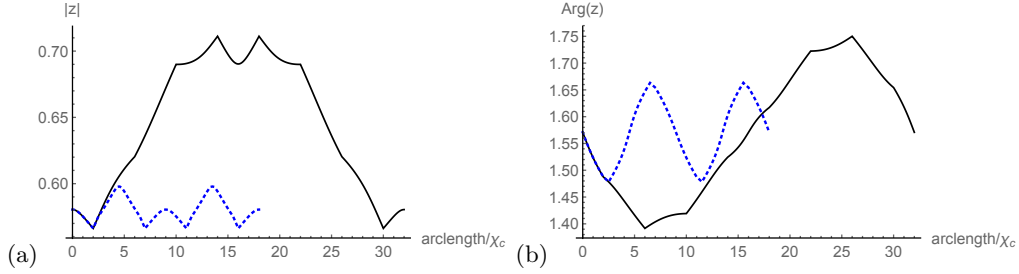


FIGURE 3. The amplitude $|\tilde{z}(\zeta)|$ (a) and the argument $\text{Arg}(\tilde{z}(\zeta))$ (b) vs. arclength in the variable ζ (scaled by χ_c) along the closed contour $0BCDA0$ shown on the left panel of Figure 2 (the contour is passed twice in the counterclockwise direction) for ODE integration (provides the analytical continuation of Stokes wave in the complex plane) of Stokes wave solution with $H/\lambda = 0.1387112446\dots$ (corresponds to $\chi_c = 3.0056373876\dots \cdot 10^{-3}$, see Table 1 of Appendix C for details on numerical Stokes wave). The contour width is $|AB| = 2|OB| = 2\chi_c$. Solid lines are for the contour height $|BC| = 4\chi_c$ (the contour $0BCDA0$ twice crosses the branch cut $[i\chi_c, i]$ in counterclockwise direction) and dotted lines are for the contour height $|BC| = \chi_c/2$ (for that height the contour $0BCDA0$ does not cross the branch cut $[i\chi_c, i]$ as well as the total arclength is smaller). It is seen that solid lines are periodic over the total arclength (two round trips around the contour $0BCDA0$ are needed to return to the initial value $z(0)$ in the first sheet of Riemann surface) compare with the half-arclength periodicity of dotted lines (the contour $0BCDA0$ is located in the first sheet only with one roundtrip sufficient to return to the initial value $z(0)$).

imaginary axis. The existence of these off-axis singularities are closely related to the analysis of Section 8. They are located significantly more far away from the origin than the on-axis $\zeta = \pm i\chi_c$ singularities. These singularities appear at each sheet starting from the third one in pairs located symmetrically with respect to the imaginary axis as schematically shown in Figure 2. The symmetric location of pairs of singularities are required from the symmetry condition

$$\bar{z}(-\zeta) = -z(\zeta). \quad (5.2)$$

That symmetry condition results from the symmetry $y(x) = y(-x)$ of Stokes wave in physical variables. The location of the first pair of off-axis square root singularities at $\zeta = \bar{\zeta}_{c_1}$ and $\zeta = -\zeta_{c_1}$ is schematically shown in the third panel of Figure 2. By adaptively increasing the horizontal and vertical sizes of the contour $ABEFA$ of Figure 2, we found that for $\chi_c \ll 1$ the first pair of off-axis square root singularities are located in the third sheet at $\zeta = \bar{\zeta}_{c_1}$ and $\zeta = -\zeta_{c_1}$ with

$$\bar{\zeta}_{c_1} \simeq (17.1719 - i10.7734)\chi_c. \quad (5.3)$$

Other off-axis pairs are located even more far away both from the real and imaginary axes as schematically shown in Figure 2. Branch cuts for all off-axis singularities are chosen to be extended horizontally as shown by dashed lines in the two right panels of Figure 2. For $|A0|, |OB| \lesssim 17.1719\chi_c$, one can use the same contour as in the left panel for all sheets. However, for larger values of $|A0|, |OB|$ one has to bypass off-diagonal singularities as shown in the two right panels of Figure 2 to keep the enumeration of the sheets as described above (based on on-axis $\zeta = \pm i\chi_c$ singularities). The number of off-axis branch points grows with the increase of the sheet number. We also performed double integration over closed contours around multiple off-axis singularities and found that each of them is the square root branch point.

By-product of ODE integration of this section is that one can also calculate the jump $-2\pi\rho(\chi)$ (see equation (2.18)) at the branch cut of the first sheet with the high precision.

E.g. one can start ODE integration at $\zeta = 0$ in the first sheet and integrate until reaching a small neighborhood of $\zeta = i\chi_c$ without crossing the branch cut $\zeta \in [i\chi_c, i]$. After that one can integrate ODE independently along two line segments $\zeta = [\pm\epsilon + i\chi_c, \pm\epsilon + i]$, $\epsilon \rightarrow 0$ and calculate a difference between these two integrations recovering $\rho(\chi)$ with the precision of our simulations $\sim 10^{-26}$. A comparison of that high precision $\rho(\chi)$ with the numerical approximation of $\rho(\chi)$ obtained in Part I from the continuous limit of Padé approximation (see Figs. 6b, 7 and 8 in Part I) confirmed the numerical error order estimates of Section 4.2 of Part I. Also we found that equations (4.6)-(4.10) are also in the excellent agreement with the numerical values of $\rho(\chi)$ confirming the asymptotical analysis of Section 4.

ODE of the type (3.4) was numerically integrated in Ref. Tanveer (1991) based on the Taylor series representation of Stokes wave in the physical sheet (the additional conformal mapping from the unit disk used in Ref. Tanveer (1991) into the half-plane \mathbb{C}^- of ζ (1.6) makes that Taylor series similar to the Fourier series representation of Part I (Dyachenko *et al.* 2016)). That representation allowed Ref. Tanveer (1991) for the first time to extend the numerical integration into the upper half \mathbb{C}^+ of the second Riemann sheet and demonstrate the existence of the square root branch point there. Thus a numerical ODE integration of Ref. Tanveer (1991) is similar to our first step of this Section restricted to \mathbb{C}^+ only.

Note that it was assumed throughout this Section that any crossing by the ODE integration contour of both $[i, i\infty]$ and $[-i\infty, -i]$ is avoided. Such crossing would be harmless in the first sheet because of 2π -periodicity of $\tilde{z}(w)$. However, starting from the second sheet, $\tilde{z}(w)$ is generally non-periodic in w . Thus the branch cuts $[i, i\infty]$ and $[-i\infty, -i]$ cannot be ignored any more contrary to the case of the first sheet case discussed in the Introduction. It implies that a crossing of these branch cut provides the additional sheets of Riemann surface. We however do not explore these sheets here because they have the distance 1 from the real axis in ζ plane for any value of χ_c thus not contributing to the formation of the limiting Stokes wave.

6. Series expansions at $\zeta = \pm i\chi_c$ and structure of Riemann surface for Stokes wave

Equation (3.1) together with the definition (2.17) shows that singularities at $\zeta = \pm i\chi_c$ are coupled through complex conjugation. We found in Part I (Dyachenko *et al.* 2016) that there is only one singularity (a square root branch point) in the first (physical) sheet of Riemann surface which corresponds to the finite complex w plane. In addition, there is a singularity at $\zeta = i$ which is the complex infinity $w = i\infty$ and is discussed in Section 4. Following Part I we chose the line segment $[i\chi_c, i]$ as the branch cut connecting these two singularities in the first sheet of Riemann surface as sketched on the left panel of Figure 1. Singularity at $\zeta = -i\chi_c$ is not allowed in the first sheet because z is analytic in the fluid domain $w \in \mathbb{C}^-$.

Consider the expansions in l th sheet of Riemann surface

$$z_{l,+}(\zeta) = \sum_{j=0}^{\infty} i e^{ij\pi/4} a_{+,l,j} (\zeta - i\chi_c)^{j/2}, \quad l = 1, 2, \dots, \quad (6.1)$$

and

$$z_{l,-}(\zeta) = \sum_{j=0}^{\infty} i e^{-ij\pi/4} a_{-,l,j} (\zeta + i\chi_c)^{j/2}, \quad l = 1, 2, \dots, \quad (6.2)$$

where subscripts “+” and “-” mean expansions at $\zeta = i\chi_c$ and $\zeta = -i\chi_c$, respectively. Here the branch cuts of $(\zeta - i\chi_c)^{1/2}$ and $(\zeta + i\chi_c)^{1/2}$ are assumed to extend from $\zeta = i\chi_c$ upwards and from $\zeta = -i\chi_c$ downwards, respectively as shown in Figure 1. Often a location of the branch cut of square root is taken on the negative real axis of the argument. To use that standard agreement about a location of the branch cut, one can replace $(\zeta - i\chi_c)^{j/2}$ and $(\zeta + i\chi_c)^{j/2}$ in equations (6.1) and (6.2) by $(-i)^{j/2}(i\zeta + \chi_c)^{j/2}$ and $i^{j/2}(-i\zeta + \chi_c)^{j/2}$, respectively.

Following Section 5, we enumerate sheets of Riemann surface according to the branch points $\zeta = \pm i\chi_c$ as follows. A crossing of the branch cut $[i\chi_c, i]$ in the counterclockwise direction means going from $l = 2n - 1$ th sheet of Riemann surface to $l = 2n$ th sheet with $n = 1, 2, \dots$. Case $l = 1$ corresponds to the physical sheet of Riemann surface. Similarly, crossing of a branch cut $[-i\chi_c, -i]$ in the counterclockwise direction means going from $l = 2n$ th sheet of Riemann surface to $l = 2n + 1$ sheet with $n = 1, 2, \dots$. Plugging expansions (6.1) and (6.2) into equation (3.1) and collecting terms of the same order of $(\zeta \pm i\chi_c)^{j/2}$ result in the following relations

$$\begin{aligned}
a_{-,2n,1} &= 0, \\
a_{-,2n,2} &= \frac{-2}{1 - \chi_c^2}, \\
a_{-,2n,3} &= \frac{16c^2}{3(1 - \chi_c^2)^2 a_{+,2n-1,1}(c^2 - a_{+,2n-1,0} - a_{-,2n,0})}, \\
a_{-,2n,4} &= \frac{2\chi_c}{(1 - \chi_c^2)^2} + \frac{4c^2}{(1 - \chi_c^2)^2(c^2 - a_{+,2n-1,0} - a_{-,2n,0})^2} \\
&\quad - \frac{8c^2[2 + (-1 + \chi_c^2)a_{+,2n-1,2}]}{(1 - \chi_c^2)^3 a_{+,2n-1,1}^2(c^2 - a_{+,2n-1,0} - a_{-,2n,0})}, \\
&\dots
\end{aligned} \tag{6.3}$$

for $n \geq 1$ and

$$\begin{aligned}
a_{+,2n+1,1} &= -\frac{16c^2}{3(1 - \chi_c^2)^2 a_{-,2n,3}(c^2 - a_{-,2n,0} + a_{+,2n+1,0})}, \\
a_{+,2n+1,2} &= \frac{2}{1 - \chi_c^2} + \frac{128c^4}{9(1 - \chi_c^2)^4 a_{-,2n,3}^2(c^2 - a_{-,2n,0} - a_{+,2n+1,0})^3} \\
&\quad + \frac{32c^2[-2\chi_c + (1 - \chi_c^2)^2 a_{-,2n,4}]}{9(1 - \chi_c^2)^4 a_{-,2n,3}^2(c^2 - a_{-,2n,0} - a_{+,2n+1,0})}, \\
a_{+,2n+1,3} &= \dots, \\
&\dots
\end{aligned} \tag{6.4}$$

for $n \geq 1$.

One cannot take $n = 0$ in equation (6.4) which corresponds to $l = 1$ (the physical sheet of Riemann surface). This special case has to be considered separately because in the physical sheet there is no singularity at $\zeta = -i\chi_c$ (no singularity inside fluid domain). It implies that

$$a_{-,1,2j+1} = 0 \quad \text{for } j = 0, 1, 2, \dots \tag{6.5}$$

Solving equations (6.1), (6.2) and (3.1) for $l = 1$ with the series expansion at $\zeta = -i\chi_c$

subject to the condition (6.5) results in the following expressions

$$\begin{aligned}
a_{+,1,0} &= c^2 - a_{-,1,0}, \\
a_{+,1,1} &= \frac{-2^{3/2}c}{(1 - \chi_c^2)^{1/2} [(2 + (1 - \chi_c^2)a_{-,1,2})]^{1/2}}, \\
a_{+,1,2} &= \frac{4}{3(1 - \chi_c^2)} - \frac{a_{-,1,2}}{3}, \\
a_{+,1,3} &= -\frac{[2 + (1 - \chi_c^2)a_{-,1,2}]^{5/2}}{2^{1/2}18c(1 - \chi_c^2)^{3/2}} \\
&\quad + \frac{2^{1/2}c [2\chi_c - 2\chi_c(-1 + \chi_c^2)a_{-,1,2} + (-1 + \chi_c^2)^2 a_{-,1,4}]}{(1 - \chi_c^2)^{3/2} [2 + (1 - \chi_c^2)a_{-,1,2}]^{3/2}}, \\
a_{+,1,4} &= \dots, \\
&\dots
\end{aligned} \tag{6.6}$$

Expressions (6.6) are uniquely determined by values of c , χ_c and $a_{-,1,2j}$, $j = 0, 1, 2, \dots$, where all expressions under square roots are positive and the principle branch of all square roots is assumed. In contrast, the expressions (6.3) and (6.4) are not the unique solutions of equations (6.1), (6.2) and (3.1). In addition to the solution (6.3), one can obtain two more spurious solutions for $a_{-,2n,j}$. However, these spurious solutions do not correspond to Stokes wave. One spurious solution has $a_{-,2n,2j+1} = 0$ for $j = 1, 2, \dots$, i.e. it does not have a singularity at $\zeta = -i\chi_c$. The second spurious solution has either a radius of convergence well below χ_c or even the zero radius of convergence. Both solutions are spurious because they cannot have the same value in the region of overlap of the disks of convergence of both expansions (6.1) and (6.2). After spurious solutions for $a_{-,2n,j}$ are discarded, one obtains the unique solution (6.3) as well as the solution (6.4) $a_{+,2n+1,j}$ also turns to be uniquely defined. Another peculiar property of the solution (6.3) is that $a_{-,2n,1} = 0$ while $a_{+,2n+1,1} \neq 0$ as given by the solution (6.4).

R.h.s. of equation (6.4) provides the explicit expressions for the coefficients $a_{+,2n+1,j}$, $j = 1, 2, \dots$, for $2n + 1$ th sheet of Riemann surface through the coefficients $a_{-,2n,j_1}$, $0 \leq j_1 \leq j + 2$ at $2n$ th sheet. The only coefficient which remains unknown is the zeroth coefficient $a_{+,2n+1,0}$ for each $n \geq 1$. In a similar way, r.h.s. of equation (6.3) provides the explicit expressions for the coefficients $a_{-,2n,j}$, $j = 1, 2, \dots$, for $2n$ th sheet of Riemann surface through the coefficients $a_{+,2n-1,j_1}$, $0 \leq j_1 \leq j - 2$, $j = 1, 2, \dots$, at $2n - 1$ th sheet. The only coefficient which remains unknown is the zeroth coefficient $a_{-,2n,0}$ for each $n \geq 1$.

The explicit expressions for $a_{+,2n+1,j}$ and $a_{-,2n,j}$ turn cumbersome with the increase of j beyond values shown explicitly in equations (6.3) and (6.4). The explicit expression $a_{+,2n+1,j}$ and $a_{-,2n,j}$ were obtained with the help of symbolic computations in Mathematica 10.2 software. These expressions were used to calculate values of all coefficients $a_{+,2n+1,j}$ and $a_{-,2n,j}$ for $j \geq 1$ numerically with any desired precision (typically we used quadruple (quad) precision with 32 digits accuracy and took into account all j in the range $1 \leq j \leq 200$). The remaining coefficients $a_{-,2n,0}$ and $a_{+,2n+1,0}$ for each $n \geq 1$ as well as the numerical value of χ_c were determined by a numerical procedure which is described below in Sections 6.1 and 6.2.

Values of $a_{+,2n+2,j}$ and $a_{-,2n+1,j}$ are obtained from $a_{+,2n+1,j}$, and $a_{-,2n,j}$ by the

following relations

$$\begin{aligned} a_{+,2n+2,j} &= (-1)^j a_{+,2n+1,j}, \quad n = 0, 1, 2, \dots, \\ a_{-,2n+1,j} &= (-1)^j a_{-,2n,j}, \quad n = 1, 2, \dots, \end{aligned} \quad (6.7)$$

which immediately follows from the condition at the crossing of branch cuts.

6.1. Finding of χ_c , from matching the series expansions at $\zeta = \pm i\chi_c$ in the first sheet

Equations (6.6) determine values of $a_{+,1,j}$, $j = 0, 1, 2, \dots$ from $a_{-,1,2j}$, $j = 0, 1, 2, \dots$ thus relating the series expansions at $\zeta = -i\chi_c$ and $\zeta = i\chi_c$ at the first sheet. The series at $\zeta = -i\chi_c$ is given by equation (6.2) with $l = 1$ together with the condition (6.5). That series contains only integer powers of $\zeta + i\chi_c$. The disk of convergence $|\zeta + i\chi_c| < r$ of that series is determined by the branch point at $\zeta = i\chi_c$ which implies that the radius of convergence is $r = 2\chi_c$. The series at $\zeta = i\chi_c$ at the first sheet is given by equations (6.1), (6.6) and contains both integer and half-integer powers of $\zeta - i\chi_c$. The disk of convergence $|\zeta - i\chi_c| < r$ is determined by the branch point at $\zeta = -i\chi_c$ of the second sheet. Thus the radius of convergence is also $r = 2\chi_c$. In other words, the radius of convergence of the series (6.1), (6.6) in the physical sheet is determined by the singularity in the second (non-physical sheet).

Numerical values of the coefficients $a_{-,1,2j}$, $j = 0, 1, 2, \dots$ are immediately obtained by the differentiation of the Padé approximants of Part I for each numerical value of H/λ . Accuracy of that approximation of the coefficients $a_{-,1,2j}$ is checked by plugging these numerical values into the series (6.2) with $l = 1$ and using (6.5). For numerical evaluation that series is truncated into a finite sum

$$z_{1,-,sum}(\zeta) = \sum_{j=0}^{j_{max}} i e^{-ij\pi/4} a_{-,1,j} (\zeta + i\chi_c)^{j/2} = \sum_{j=0}^{j_{max}/2} i e^{-ij\pi/2} a_{-,1,2j} (\zeta + i\chi_c)^j, \quad (6.8)$$

where j_{max} is chosen sufficiently large to match the numerical precision of Padé approximants. It is convenient to evaluate that sum at $\zeta = 0$ which is well inside the disk of convergence $|\zeta + i\chi_c| < 2\chi_c$. It was found that $j_{max} = 200$ at $\zeta = 0$ is well sufficient to reach a numerical precision about quad precision $\sim 10^{-32}$ of simulations of Part I. That numerical value of j_{max} (sufficient to reach quad precision) is only weakly dependent on H/λ . To understand that weak dependence one can note that $|\zeta + i\chi_c|_{\zeta=0} = \chi_c$ which is one-half of the radius of convergence of the series (6.2). The asymptotics of the terms of the series (6.2) for large j is determined by the radius of convergence as follows $|a_{-,1,2j}/a_{-,1,2j+2}| \simeq 2\chi_c$. Then the truncation of the series (6.2) by the finite sum (6.8) with $j_{max} = 200$ gives the error $\sim a_{-,1,j_{max}} \chi_c^{j_{max}/2} \sim 2^{-j_{max}/2} \sim 10^{-30}$ in comparison with Padé approximation of Stokes wave at $\zeta = 0$.

It worth to note here that the number of derivatives $j_{max}/2 = 100$ which was reliably recovered above from Padé approximation is really large which demonstrates the highly superior efficiency of Padé approximation compare with Fourier series. E.g., if instead Padé approximation of Stokes wave, one uses the Fourier series representation of Stokes wave, then the number of derivatives calculated from that series with a high numerical precision would be limited to just a few (about 10-20 derivatives if the relative error ~ 1 in derivatives is allowed).

To obtain numerical values of $a_{+,1,j}$, $j = 0, 1, 2, \dots$ from equations (6.6) one also has to know the numerical value of χ_c . Part I described a numerical procedure to recover χ_c with the accuracy $\sim 10^{-10}$ which is significantly below the accuracy $\lesssim 10^{-26}$ of numerical Stokes solution itself and its Padé approximation. In this paper to greatly improve that

precision of χ_c , one sets a condition that χ_c is chosen in such a way to allow the series (6.1) to recover the value of $z(0)$ with the accuracy better than $\sim 10^{-26}$.

Similar to equation (6.8), the series (6.1) is truncated to a finite sum

$$z_{1,+,\text{sum}}(\zeta) = \sum_{j=0}^{j_{\max}} i e^{ij\pi/4} a_{+,1,j} (\zeta - i\chi_c)^{j/2}, \quad (6.9)$$

where we again choose that $j_{\max} = 200$ which is well enough to match quad precision $\sim 10^{-32}$. Contrary to equation (6.8), the sum (6.9) includes also half-integer powers of $\zeta - i\chi_c$ because $\zeta = i\chi_c$ is the square root branch point. Using equations (6.6) and (6.9) with the numerical values of $a_{-,1,2j}$, $j = 0, 1, 2, \dots$, obtained as described in the beginning of this Section, one finds in the first sheet a numerical value of $z_{1,+,\text{sum}}(0)$ for each numerical value of χ_c . Then numerical Newton (secant) iterations are performed over χ_c aiming to ensure that $z_{1,+,\text{sum}}(0)$ converges to $\simeq z_{\text{pade}}(0)$, i.e. χ_c is chosen such that $z_{1,+,\text{sum}}(0)$ recovers the value of $z_{\text{pade}}(0)$. It provides χ_c with the precision at least 10^{-26} which is limited by the precision of Padé approximation. Part I also demonstrated the calculation of Stokes wave well beyond quad precision by using variable precision arithmetics with the achieved accuracy ~ 200 digits thus increasing of accuracy for χ_c is also possible if needed. Table 1 of Appendix C provides numerical values of χ_c which correspond to Padé approximations of Stokes wave found in Part I.

6.2. Finding of $a_{+,2n+1,0}$ and $a_{-,2n,0}$ from matching the series expansions at $\zeta = \pm i\chi_c$ in the second, third etc. sheets

The procedure for finding numerical values of χ_c and $a_{+,1,j}$, $j = 0, 1, 2, \dots$ described in Section 6.1, together with equations (6.3) and (6.7), allows to immediately find $a_{-,2,j}$, $j = 1, 2, \dots$ for each given value of $a_{-,2,0}$. Similar to equations (6.8) and (6.9), a notation is used such that $z_{l,+,\text{sum}}(\zeta)$ and $z_{l,-,\text{sum}}(\zeta)$ are the finite sums corresponding to the truncation of the series $z_{l,+}(\zeta)$ (6.1) and $z_{l,-}(\zeta)$ (6.2), respectively. We assume that $j_{\max} \simeq 200$ for these finite sums in the sheets $l = 1, 2, \dots$. The numerical Newton iterations at the first step are performed over $a_{-,2,0}$ aiming to ensure that $z_{2,-,\text{sum}}(0)$ converges to $z_{2,+,\text{sum}}(0)$. At the second step, the Newton iterations allow to find $a_{+,3,0}$ by matching $z_{3,-,\text{sum}}(0)$ and $z_{3,+,\text{sum}}(0)$. In a similar way, the third, fourth etc. steps allow to find $a_{-,4,0}$, $a_{+,5,0}$, $a_{-,6,0}$, $a_{+,7,0}$, \dots . Then using equations (6.7), one obtains values of $a_{+,n,0}$ and $a_{-,n,0}$ for all positive integer n completing the analytical continuation of Stokes wave into the disks $|\zeta \pm i\chi_c| < 2\chi_c$ in the infinite number of sheets of Riemann surface.

The result of that analytical continuation was compared with the analytical continuation by ODE integration of Section 5 giving the excellent agreement which is only limited by the standard numerical accuracy $\sim 10^{-26}$ of Stokes wave in the physical sheet. Increasing that accuracy of analytical continuation is straightforward by increasing j_{\max} for the finite sums $z_{l,+,\text{sum}}(\zeta)$ and $z_{l,-,\text{sum}}(\zeta)$ (and similar by increasing the accuracy for ODE integration) provided Stokes wave precision is increased. Table 3 of Appendix C provides a sample of numerical values of $a_{-,2n,0}$, $a_{+,2n+1,0}$, for $n = 1, 2, 3$ obtained by the numerical method outlined in this Section.

7. Singularities of Stokes wave for finite values of w

Grant (1973) and Tanveer (1991) showed that the only possible singularity in the finite complex upper half-plane of the physical sheet of Riemann surface is of square root type.

This result is consistent both with the simulations of Part I (Dyachenko *et al.* 2016) and numerical integration of ODE (3.4) in Section 5.

The analysis of Tanveer (1991) is based on a version of equation (3.2) together with the assumption of the analyticity of $\bar{z}(w)$ in \mathbb{C}^+ for the first sheet of Riemann surface. Assume that one performs ODE integration in the second, third etc. sheets of Riemann surface as described in Sections 5 and 6 with $z(w)$ at the n th sheet coupled to $\bar{z}(w)$ in the $n - 1$ th sheet. Here the counting of sheets follows Section 5 and assumes that $-\pi < \text{Re}(w) < \pi$, $|\text{Im}(w)| < \infty$ for all sheets. Then the analysis of Tanveer (1991) can be immediately generalized to the n th sheet at values of $w = w_1$ such that $z(w)$ has no singularity at $w = \bar{w}_1$ in the $n - 1$ th sheet (see equation (7.16) below). Coupling of square root singularities at $\zeta = \pm i\chi_c$ which is studied in Section 6 however goes beyond the analysis of Tanveer (1991).

The series expansions of Section 6 show that square root singularities can occur at any finite values of $w = w_1$ away from the real axis. It was found in Section 6 that each square root singularity can either have a sister square root singularity at the complex conjugated point $w = \bar{w}_1$ in the same sheet or can exist without the sister singularity at $w = \bar{w}_1$ thus going beyond the case analyzed by Tanveer (1991). A question still remains if any other type (beyond square root) of coupled singularities at $w = w_1$ and $w = \bar{w}_1$ in the same sheet is possible.

Going from the first sheet to the second one, then from the second one to the third one etc., one concludes that the only way for the singularity other than square root to appear is to be coupled with the square root singularity in the previous sheet. Otherwise it would violate the above mentioned generalization of the result of Tanveer (1991) to the arbitrary sheet. Consider a general power law singularity of $z(w)$ at $w = w_1$ coupled with the square root singularity of $\bar{z}(w)$ at $w = \bar{w}_1$. We write that general singularity in terms of double series as follows

$$z(w) = \sum_{n,m} c_{n,m} (w - w_1)^{n/2+m\alpha}, \quad (7.1)$$

where α is the real constant, $c_{n,m}$ are complex constants and n, m are integers. By shifting n and m one concludes that without loss of generality one can assume that

$$0 < \alpha < 1/2. \quad (7.2)$$

After the complex conjugation, the square root singularity of $z(w)$ at $w = \bar{w}_1$ is given by the following series

$$\bar{z}(w) = \sum_{n=0}^{\infty} d_n (w - w_1)^{n/2}, \quad (7.3)$$

where d_n are the complex constants. Coupling of $z(w)$ and $\bar{z}(w)$ in equation (3.3) explains why half-integer powers $n/2$ must be taken into account in equation (7.1). It is convenient to transform from w into a new complex variable

$$q \equiv (w - w_1)^{1/2}. \quad (7.4)$$

Equation (3.3) for the new variable q takes the following form

$$z_q = \frac{4q^2 c^2}{\bar{z}_q [i(z - \bar{z}) + c^2]}. \quad (7.5)$$

The series (7.1) is then transformed into

$$z(q) = \sum_{n,m} c_{n,m} q^{n+2m\alpha}, \quad (7.6)$$

while the series (7.3) runs over integer powers,

$$\bar{z}(q) = \sum_{n=0}^{\infty} d_n q^n. \quad (7.7)$$

The series (7.6) can be also called by ψ -series, see e.g. Hille (1997). If α is the rational number then in equation (7.1) one can gather together all terms with the same power of q thus reducing equation (7.1) to Puiseux series

$$z(q) = \sum_{n=-\infty}^{\infty} \tilde{c}_n q^{2n/k}, \quad (7.8)$$

where k is the positive integer.

If one additionally restricts that there is no essential singularity at $q = 0$ then one has to replace (7.6) with the truncated series

$$z(q) = \sum_{n \geq n_0, m \geq m_0} c_{n,m} q^{n+2m\alpha}, \quad (7.9)$$

for the integer constants n_0 and m_0 . Plugging in equations (7.7) and (7.9) into the Stokes wave equation (7.5), moving the denominator to the l.h.s. in equation (7.5) and collecting terms with the same power of q , starting from the lowest power, one obtains that 2α must be integer for any values of n_0 and m_0 and all values of d_n . Thus no new solutions in the form (7.9) exists beyond what was found in Section 6.

One can also study singularities using the classification of movable and fixed singularities in nonlinear ODEs of 1st order in the general form $z_q = f(q, z)$ (see e.g. Golubev (1950); Hille (1997); Ince (1956)). Position of fixed singularities for the independent complex variable q is determined by the properties of ODE, i.e. by singularities of the function $f(q, z)$. In contrast, the position of movable singularity is not fixed but typically is determined by an arbitrary complex constant. To analyze singularities, it is convenient to introduce a new unknown

$$\xi(q) \equiv \frac{1}{i(z - \bar{z}) + c^2}. \quad (7.10)$$

Then equation (7.5) takes the following form

$$\xi_q = i\bar{z}_q \xi^2 - \frac{4iq^2 c^2 \xi^3}{\bar{z}_q}, \quad (7.11)$$

where one reminds that $\bar{z}(q)$ is assumed to be known and is determined by $z(\bar{q})$ from the previous sheet of Riemann surface. Equation (7.11) has a cubic polynomial r.h.s in ξ which ensures that it has a movable square root singularity

$$\xi = \sum_{n=-1}^{\infty} c_n (q - C)^{n/2}, \quad (7.12)$$

provided $C \neq 0$, $\bar{z}_q(C) \neq 0$ (see e.g. Golubev (1950); Hille (1997); Ince (1956)), where c_n and C are the complex constants. Using equations (7.4), (7.10) and the condition

$C \neq 0$, one recovers the expansion (7.3) with w_1 replaced by $w_1 + C^2$ thus the movable singularity (7.12) is reduced to the square root singularity in w .

Equation (7.11) has a fixed singularity at $q = 0$ provided $\bar{z}_q(0) \neq 0$. To show that one uses a new unknown $\psi \equiv 1/\xi$ to transform equation (7.11) into

$$\psi_q = \frac{-i\bar{z}_q^2\psi + 4iq^2c^2}{\bar{z}_q\psi}, \quad (7.13)$$

which has 0/0 singularity in r.h.s. for $q = \psi = 0$ satisfying the criteria for the existence of fixed singularity (see Golubev (1950); Hille (1997)).

Consider now a particular case $\bar{z}_q(0) = 0$ and $\bar{z}_{qq}(0) \neq 0$ which corresponds to the expansion (6.3). One can define a new function

$$g(q) \equiv \frac{\bar{z}_q}{q}, \quad g(0) \neq 0 \quad (7.14)$$

and rewrite equation (7.13) as follows

$$\psi_q = \frac{-iqg(q)^2\psi + 4iqc^2}{g(q)\psi}, \quad (7.15)$$

Generally this equation still has a fixed singularity because of 0/0 singularity in r.h.s.. However, in a particular case when $g(q)$ is the even function of q , i.e. one can define the function $\tilde{g}(q^2) \equiv g(q)$ which is analytic in the variable $\tilde{q} \equiv q^2$ at $q = 0$. This case means that $z(w)$ is analytic at $w = w_1$. Then one transforms equation (7.15) into the equation

$$\psi_{\tilde{q}} = \frac{-i\tilde{g}(\tilde{q})^2\psi + 4ic^2}{2\tilde{g}(\tilde{q})\psi}, \quad (7.16)$$

which does not have a fixed singularity. Equation (7.16) together with equation (7.12) reproduces the result of Tanveer (1991) applied to all sheets of Riemann surface.

Thus the approaches reviewed in Refs. Golubev (1950); Hille (1997); Ince (1956) applied to equation (7.5) are consistent with square root singularities and the series expansions of Section 6 for all sheets of Riemann surface. However, these approaches cannot exclude the possibility of existence of other types of singularity. Note that examples given in Golubev (1950); Hille (1997); Ince (1956) also show that the existence of the fixed singularity in ODE at the point $q = 0$ does not necessary mean that the singularity occurs in the general ODE solution $z(q)$ at that point.

One concludes that a coupling of the essential singularity at $w = w_1$ with the square root singularity at $w = \bar{w}_1$ cannot be excluded neither by the series analysis used in equations (7.4)-(7.9) nor by looking at the fixed ODE singularities through equations (7.10)-(7.15). However, the simulations of Section 5 and series expansions of Section 6 clearly indicates the absence of any singularities beyond square roots in all sheets of Riemann surface for non-limiting Stokes wave in $\zeta \in \mathbb{C} \setminus ((-\infty, -i] \cup ([i, i\infty))$ (i.e. everywhere in the complex plane \mathbb{C} except the branch cuts $(-\infty, -i]$ and $[i, i\infty)$). In the first sheet the branch cuts $(-\infty, -i]$ and $[i, i\infty)$ are not significant as explained in the Introduction, and the only non-square root singularity exists at $\zeta = i$, see Section 4. It is conjectured here that non-square root singularities do not appear in all sheets of Riemann surface for $\zeta \in \mathbb{C} \setminus ((-\infty, -i] \cup ([i, i\infty))$.

As discussed at the end of Section 5, singularities are possible at the boundary of the strip $Re(w) = \pm\pi$ which corresponds to the branch cuts $[i, i\infty)$ and $[-i\infty, -i]$ in ζ plane. However, these branch cuts are separated by the distance π from the origin in w plane (or by the distance 1 in ζ plane) and they cannot explain the formation of the limiting

Stokes wave as $v_c \rightarrow 0$. The same is true for the singularity at $w \rightarrow i\infty$ ($\zeta \rightarrow i$) analyzed in Section 4.

8. Conjecture on recovering of 2/3 power law of limiting Stokes wave from infinite number of nested square root singularities of non-limiting Stokes wave as $\chi_c \rightarrow 0$

One concludes from Sections 6 and 7 that the only possibility for the formation of 2/3 power law singularity (1.1) of the limiting Stokes wave is through the merging together the infinite number of square root singularities from different sheets of Riemann surface in the limit $v_c \rightarrow 0$. The total number of square root singularities could be either finite or infinite for $v_c > 0$, both cases are compatible with the expansions of Section 6 (although the infinite number of singularities appears to hold for the generic values of the expansion coefficients of Section 6). Both numerical ODE integration of Section 5 and series expansions of Section 6 reveal that the number of sheets of Riemann surface related to singularities at $\zeta = \pm i\chi_c$ exceeds several hundreds for a wide range of numerical values $10^{-7} \lesssim \chi_c \lesssim 0.2$. It suggests that the number of sheets is infinite for all values of v_c . In any case, the number of singularities must be infinite as $v_c \rightarrow 0$.

Here a conjectured is made that the limiting Stokes wave occurs as the limit $v_c \rightarrow 0$ of the following leading order solution

$$\begin{aligned}
z &= i\frac{c^2}{2} + c_1\chi_c^{1/6}\sqrt{\zeta - i\chi_c} \\
&+ \frac{(3c)^{2/3}}{2}e^{-i\pi/6}\left[(\zeta - i\chi_c)^{1/2} + (-2i\chi_c)^{1/2}\right]\sqrt{\alpha_1\chi_c^{1/4} + \sqrt{(\zeta - i\chi_c)^{1/2} + (-2i\chi_c)^{1/2}}} \\
&\times \sqrt{\alpha_3\chi_c^{1/16} + \sqrt{\alpha_2\chi_c^{1/8} + \sqrt{\alpha_1\chi_c^{1/4} + \sqrt{(\zeta - i\chi_c)^{1/2} + (-2i\chi_c)^{1/2}}}} \\
&\times \sqrt{\alpha_{2n+1}\chi_c^{1/2^{2n+2}} + \sqrt{\alpha_{2n}\chi_c^{1/2^{2n+1}} + \sqrt{\dots + \sqrt{\alpha_1\chi_c^{1/4} + \sqrt{(\zeta - i\chi_c)^{1/2} + (-2i\chi_c)^{1/2}}}}} \\
&\times \dots + \frac{(3c)^{2/3}}{2}e^{-i\pi/6}\left[(\zeta - i\chi_c)^{1/2} + (-2i\chi_c)^{1/2}\right]\sqrt{\tilde{\alpha}_1\chi_c^{1/4} + \sqrt{(\zeta - i\chi_c)^{1/2} + (-2i\chi_c)^{1/2}}} \\
&\times \sqrt{\tilde{\alpha}_3\chi_c^{1/16} + \sqrt{\tilde{\alpha}_2\chi_c^{1/8} + \sqrt{\tilde{\alpha}_1\chi_c^{1/4} + \sqrt{(\zeta - i\chi_c)^{1/2} + (-2i\chi_c)^{1/2}}}} \\
&\times \sqrt{\tilde{\alpha}_{2n+1}\chi_c^{1/2^{2n+2}} + \sqrt{\tilde{\alpha}_{2n}\chi_c^{1/2^{2n+1}} + \sqrt{\dots + \sqrt{\tilde{\alpha}_1\chi_c^{1/4} + \sqrt{(\zeta - i\chi_c)^{1/2} + (-2i\chi_c)^{1/2}}}}} \\
&\times \dots + \text{h.o.t.}, \tag{8.1}
\end{aligned}$$

which is the infinite product of increasingly nested square roots. This conjecture was first presented at the conference talk Lushnikov *et al.* (2015). Equation (8.1) has two terms with nested roots, one with nonzero complex constants $\alpha_1, \alpha_2, \alpha_3, \alpha_4, \dots$ and another with nonzero complex constants $\tilde{\alpha}_1, \tilde{\alpha}_2, \tilde{\alpha}_3, \tilde{\alpha}_4, \dots$ which are related through complex

conjugation as follows

$$\tilde{\alpha}_1 = \bar{\alpha}_1 e^{-i\pi/4}, \quad \tilde{\alpha}_2 = \bar{\alpha}_1 e^{-i\pi/8}, \dots, \quad \tilde{\alpha}_n = \bar{\alpha}_n e^{-i\pi/2^{n+1}}, \dots \quad (8.2)$$

All these constants including another complex constant c_1 are of the order $O(1)$ independent of χ_c . The relations (8.2) ensures that the symmetry condition (5.2) is satisfied.

At $\zeta \gg \chi_c$ one obtains from equation (8.1) using the asymptotic of products of all square roots that

$$z \propto \zeta^{1/2+1/8+1/32+1/128+\dots} = \zeta^{2/3} \quad (8.3)$$

exactly reproducing the Stokes solution (1.1) while the term $c_1 \chi_c^{1/6} \sqrt{\zeta - i\chi_c}$ vanishes as $\chi_c \rightarrow 0$. For small but finite χ_c , the limiting Stokes solution (1.1) is valid for $\chi_c \ll \zeta \ll 1$, as seen from equation (8.1). For $\zeta \sim 1$, the higher order terms denoted by h.o.t. both in equations (1.1) and (8.1), becomes important such as the term with the irrational power

$$\propto \zeta^\mu, \quad \mu = 1.4693457\dots \quad (8.4)$$

(Grant 1973; Williams 1981).

Different branches of all nested square roots in equation (8.1) choose different sheets of Riemann surface following the numeration of sheets used in Section 5. In particular, the principal branch of $(\zeta - i\chi_c)^{1/2}$ in the expression $g(\zeta) \equiv (\zeta - i\chi_c)^{1/2} + (-2i\chi_c)^{1/2}$ corresponds to the first sheet. To understand that one expands $g(\zeta)$ at $\zeta = -i\chi_c$ which results in

$$g_+(\zeta) = 2(-2i\chi_c)^{1/2} + \frac{\zeta + i\chi_c}{2(-2i\chi_c)^{1/2}} + O(\zeta + i\chi_c)^2, \quad (8.5)$$

where the subscript “+” means taking the principle branch of $(\zeta - i\chi_c)^{1/2}$. For the second (negative) branch of $(\zeta - i\chi_c)^{1/2}$ one obtains that

$$g_-(\zeta) = -\frac{\zeta + i\chi_c}{2(-2i\chi_c)^{1/2}} + O(\zeta + i\chi_c)^2 \quad (8.6)$$

with the subscript “-” meaning that second branch.

The expression $g(\zeta)$ enters under the most inner square root into each term of the product in equation (8.1). Then using the expansion (8.5) one obtains that the series expansion of equation (8.1) at $\zeta = -i\chi_c$ contains only nonnegative integer powers of $\zeta + i\chi_c$ thus confirming that $z(\zeta)$ is analytic at $\zeta = -i\chi_c$. It means that the condition (6.5) is satisfied. In contrast, taking the expansion (8.6) one obtains that the series expansion of equation (8.1) at $\zeta = -i\chi_c$ is of the type (6.2) containing nonnegative half-integer powers of $\zeta + i\chi_c$ as expected for all sheets starting from the second sheet. In addition, the term $g(\zeta)$ in the square brackets in equation (8.1) ensures that $a_{-,2n,1} = 0$ as required by equation (6.3). The expansion of equation (8.1) at $\zeta = i\chi_c$ has half-integer powers of $\zeta - i\chi_c$ for both branches of $g(\zeta)$ thus being consistent with the square root singularity at $\zeta = i\chi_c$ in all sheets of Riemann surface including the first sheet in agreement with equations (6.1), (6.4) and (6.6).

Choosing two possible branches of all other nested square roots (besides the most inner square root) in equation (8.1) one obtains the expansions (6.1) and (6.2), at $\zeta = \pm i\chi_c$ with different coefficients $a_{+,l,j}$ and $a_{-,l,j}$ at each l th sheet. The values of these coefficients are determined by both values of $\chi_c, c_1, \alpha_1, \alpha_2, \alpha_3, \alpha_4, \dots$ together with the contribution from h.o.t terms in equation (8.1). One concludes that the ansatz (8.1) is consistent with the properties of non-limiting Stokes wave studied in this paper which motivates the conjecture (8.1). Also coefficients $\alpha_1, \alpha_2, \alpha_3, \dots$ determine additional square root branch points which are located away from the imaginary axis at distance larger than χ_c from

the origin in the third and higher sheets of Riemann surface. Values of these coefficients can be determined from the locations of branch points thus independently recovered from ODE integration similar to described in Section 5 (see also Section 8.1 for the example of recovering of α_1).

8.1. Numerical verification of the conjecture

Now we provide a numerical demonstration of the efficiency of the conjecture (8.1) by using the simplest nontrivial approximation of equation (8.1) which takes into account only the three-fold nested roots as follows

$$\begin{aligned}
z \simeq & \left(i \frac{c^2}{2} + c_0 \chi_c^{2/3} \right) + c_1 \chi_c^{1/6} \sqrt{\zeta - i \chi_c} + c_2 \zeta \\
& + c_3 \chi_c^{1/24} \left[(\zeta - i \chi_c)^{1/2} + (-2i \chi_c)^{1/2} \right] \sqrt{\alpha_1 \chi_c^{1/4} + \sqrt{(\zeta - i \chi_c)^{1/2} + (-2i \chi_c)^{1/2}}} \\
& + \bar{c}_3 e^{-\frac{3i\pi}{8}} \chi_c^{1/24} \left[(\zeta - i \chi_c)^{1/2} + (-2i \chi_c)^{1/2} \right] \sqrt{\bar{\alpha}_1 e^{-\frac{i\pi}{4}} \chi_c^{1/4} + \sqrt{(\zeta - i \chi_c)^{1/2} + (-2i \chi_c)^{1/2}}}
\end{aligned} \tag{8.7}$$

where we added the term $c_2 \zeta$ as well the constants c_0 , c_2 and c_3 to approximate the neglecting of other nested roots (which includes $\alpha_2, \alpha_3, \dots$) in comparison with equation (8.1). In other words, we approximate all more than three-fold nested roots in equation (8.1) by Taylor series expansion keeping only the constant and linear terms in ζ in that expansion. The constant terms result in adding the constants c_3 and \bar{c}_3 in front of nested roots as well as in the small correction $c_0 \chi_c^{2/3}$ to the constant term $ic^2/2$ of equation (8.1). The linear terms result in the appearance of the constant c_2 replacing higher order nested roots of equation (8.1). Also the factor $\bar{c}_3 e^{-\frac{3i\pi}{8}}$ ensures the symmetry (5.2) and the additional scaling $\chi_c^{1/24}$ provides for $\zeta \sim \chi_c$ the same total scaling $\propto \chi_c^{2/3}$ of the nested square roots of equation (8.7) as in equation (8.1). The approximation (8.1) can be valid only up to moderately large values of $Re(\zeta) = \zeta$ (a comparison with equation (8.1) suggests that it could be valid up to values of ζ in about several tens of χ_c after that higher order nested roots must come into play).

To find the numerical values of α_1 , c_0 , c_1 , c_2 and c_3 without any fit we use the following procedure. At the first step we determine from the contour integration of Section 5 the location (5.3) of the first pair of off-axis square root singularities (located at $\zeta = \bar{\zeta}_{c_1}$ and $\zeta = -\zeta_{c_1}$). Then we solve equation $\alpha_1 \chi_c^{1/4} + \sqrt{(\bar{\zeta}_{c_1} - i \chi_c)^{1/2} + (-2i \chi_c)^{1/2}} = 0$ (corresponds to the zero under three-fold square root in equation (8.1)) in the third sheet of the Riemann surface which together with (5.3) gives that

$$\alpha_1 \simeq -0.0955383 - i 1.8351. \tag{8.8}$$

Note that the second square root $\zeta = -\zeta_{c_1}$ (symmetric with respect to the imaginary axis) is ensured by the similar term with $\bar{\alpha}_1 e^{-\frac{i\pi}{4}}$ in equation (8.7). At the second step we expand equation (8.1) in the first sheet of Riemann surface in powers of $(\zeta - i \chi_c)^{1/2}$. After that we match the first five coefficients of that expansion to the analytical expressions of the coefficients $a_{+,1,j}$, $j = 1, \dots, 5$, of the expansion (6.6) obtained in Section 6. That matching results in the explicit expressions for c_0 , c_1 , c_2 and c_3 . E.g., for Stokes wave with $\chi_c = 2.9691220994 \dots \cdot 10^{-7}$ (corresponds to the last line of table 1 of Appendix C, see that Appendix for more details on the numerical Stokes wave) we obtain that $c_0 = i 17.1920 \dots$, $c_1 = e^{-i\pi/4} 3.81499 \dots$, $c_2 = -1.8779 \dots$ and $c_3 = 1.42696 \dots - i 1.8849 \dots$

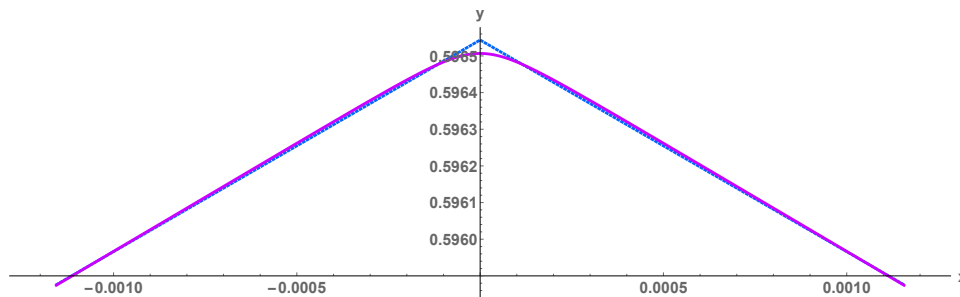


FIGURE 4. A comparison of the limiting Stokes wave (dotted line) with equation (8.7) and the numerical solution for Stokes wave (last two of these are shown by the single solid line because they are visually indistinguishable with maximum difference between them $\simeq 4 \cdot 10^{-6}$) for $\chi_c = 2.9691220994 \dots \cdot 10^{-7}$. Solid line corresponds to $-50\chi_c \leq \zeta \leq 50\chi_c$.

Changing of χ_c by several orders of magnitude results in changing these coefficients only within the range 5 – 10%.

We demonstrated the efficiency of the obtained numerical values of c_0 , c_1 , c_2 and c_3 in two independent ways. In the first way, it was checked that the coefficients $a_{+,1,j}$ of equation (6.6) for $j = 6, \dots$ are well reproduced (within 4% and 7% accuracy for $j \leq 10$ and $j \leq 100$, respectively) by the expansion of equation (8.7) with the same numerical values of c_0 , c_1 , c_2 and c_3 . It implies that the approximate expression (8.7) captures the significant property of the convergence of the series (6.6) rather than being just the match of a few first terms of that series. The second way of efficiency demonstration is provided in Figure 4, where the excellent agreement is shown between the numerical solution of Stokes wave from Part I (Dyachenko *et al.* 2016) and the expression (8.7) for $-50\chi_c \leq \zeta \leq 50\chi_c$. That range of ζ is far beyond the disk of convergence $|\zeta - i\chi_c| < 2\chi_c$ of the series (6.6).

9. Concluding remarks

In summary, it was found that the Riemann surface corresponding to non-limiting Stokes wave consists of the infinite number of sheets corresponding to the infinite number of square root branch points located at $\zeta = \pm i\chi_c$ in all sheets except the first sheet. The first (physical) sheet has only one singularity at $\zeta = i\chi_c$ while avoiding singularity at $\zeta = -i\chi_c$ which ensures that Stokes wave represents the analytical solution inside the fluid domain. Two ways of analytical continuation into all these sheets were used, the first one is based on ODE integration of Section 5 and the second one is based on the coupled series expansions (6.1)-(6.6) in half-integer powers at $\zeta = \pm i\chi_c$.

To go beyond the disks of convergence $|\zeta \pm i\chi_c| < 2\chi_c$ of the series expansions (6.1)-(6.6), it is conjectured in Section 8 that the leading order form of non-limiting Stokes wave consists of the infinite number of nested square roots (8.1). These nested square roots can recover the series expansions (6.1)-(6.6) within their disks of convergence $|\zeta \pm i\chi_c| < 2\chi_c$. For $|\zeta \pm i\chi_c| \gg \chi_c$, well beyond these disks of convergence, the asymptotic (8.3) is valid thus ensuring that the nested square roots form 2/3 power law singularity of the limiting Stokes wave in the limit $\chi_c \rightarrow 0$.

There are two other infinite sequences of Riemann sheets resulting from (a) off-axis square root singularities in the third and higher sheets of Riemann surface as analyzed in Sections 5 and 8, and (b) the singularity at $\zeta = i$ (corresponds to $w = i\infty$) which involves logarithms as analyzed in Section 4. However, these extra sheets do not contribute to

the qualitative change of power law singularity from 1/2 (non-limiting Stokes wave) to 2/3 (limiting Stokes wave) near the origin as given by the asymptotic (8.3). However, these extra sheets are expected to be important for the analysis of Stokes wave for $\zeta \sim 1$, where the higher order terms becomes important such as the term (8.4) with the irrational power (Grant 1973; Williams 1981). The analysis of these terms is beyond the scope of this paper. These terms might be also essential to answer the question left open by Refs. Longuet-Higgins & Fox (1977); McLeod (1997) about whether the number of oscillations in the slope of a non-limiting Stokes wave increases to infinity as non-limiting Stokes wave approaches its limiting form. Note that these oscillations vanish for the limiting Stokes wave as was proven in Ref. Plotnikov & Toland (2004).

Appendix A. Equivalence of two form of equation for Stokes wave

In this Appendix we show that both forms (2.1) and (3.1) of equation for Stokes wave are equivalent to each other. Then Section 2 implies that equations (2.13) and (2.22) are also equivalent to equations (2.1) and (3.1). Equation (2.1) was obtained by Dyachenko *et al.* (1996) while equation (3.1) in slightly different forms was used by numerous authors including Grant (1973); Longuet-Higgins & Fox (1977); Schwartz (1974); Stokes (1880*b*); Williams (1981) and Tanveer (1991). Appendix B explains the derivation of equation (3.1) starting from basic equations of the potential flow of ideal fluid with free surface.

Applying the Hilbert operator \hat{H} (2.2) to equation (2.1) and using the relations (2.14) and (2.15) one obtains that

$$c^2 \tilde{x}_u - yx_u + \hat{H}[yy_u] = 0, \quad (\text{A } 1)$$

which is equivalent to equation (2.13). We define a new variable

$$f \equiv -\hat{H}[yy_u] \quad (\text{A } 2)$$

and split it into two functions

$$f = f^+ + f^-, \quad (\text{A } 3)$$

using equations (2.4), (2.7), (2.8) and (2.9) such that f^+ and f^- are the functions which are analytic in upper half-plane \mathbb{C}^+ and lower complex half-plane \mathbb{C}^- of w , respectively. Note that the zeroth harmonic $f_0 = 0$ as it follows from the definition (A 2). Taking the linear combination of f and $\hat{H}f$, using equations (2.1), (A 1) and (A 2), one finds that

$$x_u \hat{H}f + y_u f = c^2 \tilde{x}_u y_u. \quad (\text{A } 4)$$

Using obvious relations

$$x_u = \frac{1}{2}(z_u + \bar{z}_u), \quad y_u = \frac{1}{2i}(z_u - \bar{z}_u) \quad (\text{A } 5)$$

together with equations (A 3), (2.10) one obtains from equation (A 4) that

$$\bar{z}_u f^+ - z_u f^- = \frac{c^2}{4} (\bar{z}_u^2 - z_u^2). \quad (\text{A } 6)$$

Recalling that z_u is analytic in \mathbb{C}^- and, respectively, \bar{z}_u is analytic and in \mathbb{C}^+ , we apply the projector (2.11) to equation (A 6) and find that

$$\begin{aligned} f^+ &= \frac{c^2}{4} \frac{\bar{z}_u^2}{\bar{z}_u}, \\ f^- &= \frac{c^2}{4} \frac{z_u^2}{z_u}, \end{aligned} \quad (\text{A } 7)$$

where $z_u \neq 0$ in \mathbb{C}^- and $\bar{z}_u \neq 0$ in \mathbb{C}^+ because $z(w)$ is the conformal transformation in \mathbb{C}^- .

Then using equations (A 1), (A 2), (A 3), (A 5) and (A 7) with some algebra we recover equation (3.1) thus completing the proof of its equivalence to equation (2.1). Note that the mean-zero elevation condition (2.15) is essential in that proof making equation (A 1) valid. Shifting of the origin in y -direction would result in the nonzero value of the mean elevation $y_{mean} \equiv \frac{1}{2\pi} \int_{-\pi}^{\pi} \eta(x, t) dx$. Then one would have to replace y by $y - y_{mean}$ in equation (3.1). E.g. Tanveer (1991) took $y_{mean} = -c^2/2$. A similar choice $y_{mean} = -c^2/2$ was used by Grant (1973), Williams (1981) and Plotnikov (1982) up to trivial scaling of parameters.

Appendix B. Stokes wave in the rest frame and in the moving frame

Starting from Stokes (1880*b*), it has been common to write Stokes wave equation at moving reference frame in transformed form with a velocity potential and a stream function used as independent variables, see e.g. Grant (1973); Williams (1981) and Tanveer (1991). The purpose of this Appendix is to relate that traditional form of Stokes wave equation to another form used by Dyachenko *et al.* (1996); Zakharov *et al.* (2002).

In physical coordinates (x, y) a velocity \mathbf{v} of two dimensional potential flow of inviscid incompressible fluid is determined by a velocity potential $\Phi(x, y, t)$ as $\mathbf{v} = \nabla\Phi$. Here x is the horizontal axis and y is the vertical axis pointing upwards. The incompressibility condition $\nabla \cdot \mathbf{v} = 0$ results in the Laplace equation

$$\nabla^2\Phi = 0 \tag{B1}$$

inside fluid $-\infty < y < \eta(x, t)$. The Laplace equation is supplemented by the dynamic boundary condition (the Bernoulli equation at the free surface $y = \eta(x, t)$)

$$\left(\frac{\partial\Phi}{\partial t} + \frac{1}{2} (\nabla\Phi)^2 \right) \Big|_{y=\eta(x,t)} + \eta = 0 \tag{B2}$$

and the kinematic boundary condition

$$\frac{\partial\eta}{\partial t} = \left(-\frac{\partial\eta}{\partial x} \frac{\partial\Phi}{\partial x} + \frac{\partial\Phi}{\partial y} \right) \Big|_{y=\eta(x,t)} \tag{B3}$$

at the free surface. In our scaled units, the acceleration due to gravity is $g = 1$. We define the boundary value of the velocity potential as $\Phi(x, y, t)|_{y=\eta(x,t)} \equiv \psi(x, t)$. Equations (B 1), (B 2) and (B 3), together with the decaying boundary condition at large depth

$$\Phi(x, y, t)|_{y \rightarrow -\infty} = 0 \tag{B4}$$

form the closed set of equations. Equation (B 4) implies that the rest frame is used such that there is no average fluid flow deep inside fluid. See also Part I (Dyachenko *et al.* 2016) for more details on basic equations of free surface hydrodynamics.

Consider the stationary waves moving in the positive x direction (to the right) with the constant velocity c so that

$$\begin{aligned} \Phi &= \Phi(x - ct, y), \\ \eta &= \eta(x - ct). \end{aligned} \tag{B5}$$

It was obtained in Ref. Dyachenko *et al.* (1996) (see also Part I (Dyachenko *et al.*

2016)) that $\Psi = -c\hat{H}y = c\tilde{x}$, where \hat{H} is the Hilbert transform (2.2). Respectively, $\hat{H}\Psi = cy$. The complex velocity potential Π at the free surface is given by

$$\Pi = \Psi + i\hat{H}\Psi = c(x + iy - u). \quad (\text{B } 6)$$

The analytical continuation of (B 6) into the lower complex half-plane $w \in \mathbb{C}^-$ is given by

$$\Pi = c(z - w) = c\tilde{z}. \quad (\text{B } 7)$$

We perform a Galilean transformation to a frame moving with the velocity c in the positive direction with the new horizontal coordinate $x' \equiv x - ct$ so that the velocity potential and the surface elevation turn time-independent as $\Phi(x')$ and $\eta(x')$, respectively. Alternatively, one can also define a velocity potential in the moving frame as $\tilde{\Phi}(x', y) = \tilde{\Phi}(x - ct, y)$ such that

$$\Phi = (x - ct)c + \tilde{\Phi}(x - ct, y). \quad (\text{B } 8)$$

Then equation (B 2) results in

$$\frac{1}{2} \left(\nabla \tilde{\Phi} \right)^2 \Big|_{y=\eta(x-ct)} + \left(\eta - \frac{c^2}{2} \right) = 0 \quad (\text{B } 9)$$

and (B 3) gives

$$\left(-\frac{\partial \eta}{\partial x} \frac{\partial \tilde{\Phi}}{\partial x} + \frac{\partial \tilde{\Phi}}{\partial y} \right) \Big|_{y=\eta(x-ct)} = 0. \quad (\text{B } 10)$$

The decaying boundary condition (B 4) is replaced by

$$\tilde{\Phi}(x', y)|_{y \rightarrow -\infty} = -c. \quad (\text{B } 11)$$

Equations (B 9), (B 10) and (B 11) are the standard equations for Stokes wave in the moving frame, see e.g. Grant (1973); Williams (1981). Often small variations of equations (B 9), (B 10) and (B 11) are used such as a trivial shift of the origin in the vertical direction $\eta - \frac{c^2}{2} \rightarrow \eta$, assuming that Stokes wave moves in negative direction (to the left) and rescaling c to one (then the spatial period 2π is also rescaled) as was done in Grant (1973).

Similar to (B 8), we define the stream function in two forms, $\Theta(x')$ and $\tilde{\Theta}(x')$ (in the rest frame and in the moving frame, respectively) as follows

$$\Theta = cy + \tilde{\Theta}(x - ct, y). \quad (\text{B } 12)$$

Using equations (B 8) and (B 12) one obtains that correspondingly, that two forms of the complex velocity potential, $\Pi(x')$ and $\tilde{\Pi}(x')$, are given by

$$\Pi = \Phi + i\Theta = cz - c^2t + \tilde{\Phi} + i\tilde{\Theta}. \quad (\text{B } 13)$$

A comparison of (B 7) and (B 13) reveals that

$$\tilde{\Pi} = \tilde{\Phi} + i\tilde{\Theta} = -c(w - ct) = -cw', \quad (\text{B } 14)$$

where $w' \equiv w - ct$. Thus $\tilde{\Pi}$ is the same as w' (up to the multiplication on $-c$) which explains why using the velocity potential $\tilde{\Phi}$ and the stream function $\tilde{\Theta}$ as independent variables in Refs. Grant (1973); Stokes (1880b); Williams (1981) is equivalent to using w' as the independent variable in Ref. Dyachenko *et al.* (1996). The difference between Π

and $\tilde{\Pi}$ is reflected by the boundary conditions (B 4) and (B 11) such that for Π the fluid at infinite depth has a zero velocity while for $\tilde{\Pi}$ that velocity is $-c$ in the x -direction. A technical advantage of working with Π instead of $\tilde{\Pi}$ in Ref. Dyachenko *et al.* (1996) is that the decaying boundary condition (B 4) allows to relate real and imaginary parts of Π through the Hilbert transform for real values of w' as $\Theta = \hat{H}\Phi$ and $\Phi = -\hat{H}\Theta$. Equations (B 9) and (B 14) results in Stokes wave equation in the form (3.1) after we notice that $(\nabla\tilde{\Phi})^2|_{y=\eta} = \frac{|\tilde{\Pi}_u|^2}{|z_u|^2} = \frac{c^2}{|z_u|^2}$.

Appendix C. Tables for numerical values of χ_c for Stokes wave

Table 1 provides a sample of the dependence of the singularity position χ_c on the scaled wave height $H/\lambda = H/(2\pi)$ for Stokes wave. Numerical values of χ_c are obtained by the numerical procedure described in Section 6.1. The Padé approximants from Part I (Dyachenko *et al.* 2016) (these approximants are also available through the electronic attachment to Ref. Dyachenko *et al.* (2015a) and at the web link Dyachenko *et al.* (2015b)) are used for each values of H/λ . More values of χ_c for different values of H/λ are also available at the web link Dyachenko *et al.* (2015b). The accuracy of numerical values of χ_c is at least 10^{-26} which is limited by the precision of Padé approximation.

We chose parameters at 1st, 3rd and 5th lines of table 1 to correspond Stokes waves with $c = 1.03, 1.066$ and 1.086 , respectively (here the exact values of c are used). These three particular values of parameters correspond to three highest Stokes waves provided in table 1 of Ref. Tanveer (1991). Table 2 reproduces these three highest waves from table 1 of Tanveer (1991), where the position of square root branch point $\zeta = i\chi_c$ is recovered from the parameter ζ_0 of Ref. Tanveer (1991) as $\chi_c = -(1 + \zeta_0)/(1 - \zeta_0)$. Also H in Ref. Tanveer (1991) is the half-height of Stokes wave so it is divided by π in table 2. The comparison of tables 1 and 2 reveals that while all digits except the last one or two agree for two smaller values of H/λ , but the agreement looses one more digit with the increase of H/λ . It is possible that Ref. Tanveer (1991) expected that loss of numerical precision because the number of digits provided in table 1 of Tanveer (1991) decreases with the increase of H/λ .

Table 3 provides a sample of numerical values of $a_{-,2n,0}$ and $a_{+,2n+1,0}$ for four different values of χ_c corresponding to table 1. These numerical values of χ_c are obtained by the numerical procedure described in Section 6.2. For brevity only 16 digits of the numerical precision are shown.

REFERENCES

- AMICK, C. J. & FRAENKEL, L. E. 1987 On the behavior near the crest of waves of extreme form. *Trans. Amer. Math. Soc.* **299**, 273–298.
- AMICK, C. J., FRAENKEL, L. E. & TOLAND, J. F. 1982 On the Stokes conjecture for the wave of extreme form. *Acta Math.* **148**, 193–214.
- BABENKO, K. I. 1987 Some remarks on the theory of surface waves of finite amplitude. *Soviet Math. Doklady*, **35** (3), 599–603.
- BUFFONI, B., DANCER, E. N. & TOLAND, J. F. 2000 The sub-harmonic bifurcation of Stokes waves. *Arch. Ration. Mech. Anal.* **152**, 241–271.
- BUFFONI, B. & TOLAND, J. F. 2001 Dual free boundaries for Stokes waves. *C. R. Acad. Sci. Paris Sr. I Math.* **332**, 73–78.
- DYACHENKO, ALEXANDER I., KUZNETSOV, EVGENII A., SPECTOR, MICHAEL & ZAKHAROV, VLADIMIR E. 1996 Analytical description of the free surface dynamics of an ideal fluid (canonical formalism and conformal mapping). *Phys. Lett. A* **221**, 73–79.
- DYACHENKO, SERGEY A., LUSHNIKOV, PAVEL M. & KOROTKEVICH, ALEXANDER O. 2013a The complex singularity of a Stokes wave. *JETP Letters* **98** (11), 767–771.

Wave height H/λ	Singularity position χ_c
0.077390566513510100664367446945009	0.22959283981280615879703284574991
0.10042675172528485854673515635249	0.12126855832745608069685459720991
0.11396866940628458279840665192065	0.071654598419719678169515049620847
0.12063157457100181211171486096916	0.050466513002046555340085106251597
0.13046836752896146189584028585057	0.022711769117183995733113183176661
0.13871124459012593791450261565795	0.0030056373876010407473234354599642
0.14003037735536232024327827857514	0.0007999065189780408034349632263817
0.14011096764402710691403135029555	0.00069951386487208337732279647662665
0.14015101306439164612988663680930	0.00065164210434348698577048482811606
0.14033404782061154512392085005894	0.00045087566212961727243263909506818
0.14051416938624427610421738297959	0.00028427822364922236690177980170163
0.14056584420653835444977911685203	0.00024252541408812956956630147113284
0.14070850110629620828789822957203	0.00014199627497457559254018017702833
0.14074703013044272779483720282718	0.00011868402545440790157599298606945
0.14075662532618050016439516401203	0.0001131402886276901411780810604808
0.14077748818517580368147808000934	0.00010145173966680681771175565637662
0.14080831525231916769272562321913	0.000085108686515454366575393860892637
0.14083140371280991872217783523764	0.000073606496213860270898473095913984
0.14085072731982411577531399667650	0.000064475962982549833303295412314089
0.14086825990337854565346642922133	0.000056590609636696915098098733019878
0.14087792765270709969236336933758	0.00005240769363924544328892679639685
0.14088586197110133631188309127224	0.000049063815868419517646209932713057
0.14089635109209977336909824577330	0.00004476805660136311962064510052487
0.14091001709910523062648751945506	0.000039388011825703454833655362993012
0.14091839307555128402812965695553	0.000036214071851881467799287017287358
0.14092032625051507844376744407087	0.00003549506133290811208694741093295
0.14092252442341776630057428860718	0.0000346837089035969690548283554112
0.14092514757875551525458131241416	0.000033724196620161039218316518297236
0.14092738180637770768107092780251	0.000032914454078339616366407901860458
0.14093056906823728426117769727974	0.000031771329157192593064752326105744
0.14093510137194143743061264048898	0.0000301703287220913256069400404687
0.14094119430696937198416665739014	0.000028063945797678144251500481216356
0.14094867821783188240349944668053	0.000025549865907771481807832323273915
0.14095352707479979419800954052129	0.000023964796260036642282422099761643
0.14095778935504595764411825281530	0.000022600407539173053002286018858435
0.14097009565718766875950104063752	0.000018816656490602043348418618380363
0.14098407663748727496462567878823	0.00001480968355336403686583695738714
0.14100153154854889551064171690484	0.000010273655389226364040855903301072
0.14103365111671204571809985597404	3.5012288974834512273437793255939e-6
0.14105431648358048728514606849313	6.0520035443913536064479745209207e-7
0.14105777885488320816492860225696	2.9691220994639291094028846634237e-7

TABLE 1. A sample of numerical values of χ_c vs. the scaled Stokes wave height H/λ .

H/λ	c	χ_c
0.07739055	1.0300	0.22958
0.1139758	1.0660	0.071667
0.13055	1.0860	0.022769

TABLE 2. Parameters of three highest Stokes waves of Table 1 from Tanveer (1991). Units are converted to the notation of this paper with the same number of digits kept as in Ref. Tanveer (1991).

	$\chi_c = 0.12126\dots$	$\chi_c = 0.05046\dots$	$\chi_c = 0.000242\dots$	$\chi_c = 2.969\dots \times 10^{-7}$
$a_{-,2,0}$	1.947517181530394	1.332875450393561	0.616114648091185	0.5967616372529635
$a_{+,3,0}$	1.933089192507101	1.395722669719572	0.6227276830074182	0.5968472222666076
$a_{-,4,0}$	2.823744469669705	1.830765178354924	0.630550992725188	0.5969268580437934
$a_{+,5,0}$	2.715883020102187	1.841263995239744	0.6356646908933044	0.5969952862738779
$a_{-,6,0}$	3.541346294820654	2.238582675537623	0.642377214720984	0.5970622067844041

TABLE 3. A sample of numerical values of $a_{-,2n,0}$ and $a_{+,2n+1,0}$, $n = 1, 2, 3$, for different χ_c . More accurate numerical values of χ_c can be recovered from table 1.

- DYACHENKO, SERGEY A., LUSHNIKOV, PAVEL M. & KOROTKEVICH, ALEXANDER O. 2015a Branch Cuts of Stokes Wave on Deep Water. Part I: Numerical Solution and Padé Approximation. *ArXiv:1507.02784*.
- DYACHENKO, SERGEY A., LUSHNIKOV, PAVEL M. & KOROTKEVICH, ALEXANDER O. 2015b Library of Stokes waves. URL: <http://stokeswave.org>.
- DYACHENKO, SERGEY A., LUSHNIKOV, PAVEL M. & KOROTKEVICH, ALEXANDER O. 2016 Branch Cuts of Stokes Wave on Deep Water. Part I: Numerical Solution and Padé Approximation. *Studies in Applied Mathematics*, DOI: 10.1111/sapm.12128.
- DYACHENKO, SERGEY A., LUSHNIKOV, PAVEL M. & VLADIMIROVA, NATALIA 2013b Logarithmic scaling of the collapse in the critical Keller-Segel equation. *Nonlinearity* **26**, 3011–3041.
- FRAENKEL, L. E. 2007 A constructive existence proof for the extreme Stokes wave. *Arch. Ration. Mech. Anal.* **183**, 187–214.
- FRAENKEL, L. E. 2010 The behaviour near the crest of an extreme Stokes wave. *European J. Appl. Math.* **21**, 165–180.
- FRAENKEL, L. E. & HARWIN, P. J. 2010 On the local uniqueness and the profile of the extreme Stokes wave. *European J. Appl. Math.* **21**, 137–163.
- GOLUBEV, V. V. 1950 *Lectures on the Analytic Theory of Differential Equations (in Russian)*. Moscow: Gosud. Izd. Techniko-Teor. Leterat.
- GRANT, MALCOLM A. 1973 The singularity at the crest of a finite amplitude progressive Stokes wave. *J. Fluid Mech.* **59(2)**, 257–262.
- HILLE, E. 1997 *Ordinary Differential Equations in the Complex Domain*. Dover.
- INCE, EDWARD L. 1956 *Ordinary Differential Equations*. Dover.
- LONGUET-HIGGINS, M. S. & FOX, M. J. H. 1977 Theory of the almost-highest wave: the inner solution. *J. Fluid Mech.* **80(4)**, 721–741.
- LUSHNIKOV, P. M., DYACHENKO, S. A. & KOROTKEVICH, A. O. 2015 Branch cut singularity of Stokes wave on deep water. *Presentation at The Ninth IMACS International Conference on Nonlinear Evolution Equations and Wave Phenomena. University of Georgia, Athens, Georgia, USA, April 02, 2015*.
- LUSHNIKOV, PAVEL M., DYACHENKO, SERGEY A. & VLADIMIROVA, NATALIA 2013 Beyond leading-order logarithmic scaling in the catastrophic self-focusing of a laser beam in Kerr media. *Phys. Rev. A* **88**, 013845.
- MCLEOD, J. B. 1987 The asymptotic behavior near the crest of waves of extreme form. *Trans. Amer. Math. Soc.* **299**, 299–302.
- MCLEOD, J. B. 1997 The Stokes and Krasovskii conjectures for the wave of greatest height. *Stud. Appl. Math.* **98**, 311–333.
- PLOTNIKOV, P. I. 1982 A proof of the Stokes conjecture in the theory of surface waves. *Dinamika Splosh. Sredy (In Russian. English translation Stud. Appl. Math. 108:217-244 (2002))* **57**, 41–76.
- PLOTNIKOV, P. I. 1991 Nonuniqueness of solutions of a problem on solitary waves and bifurcations of critical points of smooth functionals. *Izv. Akad. Nauk SSSR Ser. Mat. (In Russian. English translation in Math. USSR-Izv. 38:1992, 333357* **55**, 339–366.
- PLOTNIKOV, P. I. & TOLAND, J. F. 2002 The Fourier coefficients of stokes waves. In *Nonlinear Problems in Mathematical Physics and Related Topics, I, Int.Math. Ser.*, pp. 303–315. New York: Kluwer/Plenum.

- PLOTNIKOV, P. I. & TOLAND, J. F. 2004 Convexity of Stokes waves of extreme form. *Arch. Ration. Mech. Anal.* **171**, 349–416.
- SCHWARTZ, LEONARD W. 1974 Computer extension and analytic continuation of Stokes' expansion for gravity waves. *J. Fluid Mech.* **62(3)**, 553–578.
- SHARGORODSKY, E. & TOLAND, J. F. 2008 Bernoulli free-boundary problems. *Mem. Amer. Math. Soc.* **196**, 349–416.
- STOKES, GEORGE G. 1847 On the theory of oscillatory waves. *Transactions of the Cambridge Philosophical Society* **8**, 441–455.
- STOKES, GEORGE G. 1880a On the theory of oscillatory waves. *Mathematical and Physical Papers* **1**, 197–229.
- STOKES, GEORGE G. 1880b Supplement to a paper on the theory of oscillatory waves. *Mathematical and Physical Papers* **1**, 314–326.
- TANVEER, S. 1991 Singularities in water waves and Rayleigh-Taylor instability. *Proc. R. Soc. Lond. A* **435**, 137–158.
- TANVEER, SALEH 2013 Analytical Approximation for 2-D Nonlinear Periodic Deep Water Waves. *arXiv:1309.5801*.
- VERNER, J. H. 2010 Numerically optimal Runge-Kutta pairs with interpolants. *Numerical Algorithms* **53**, 383–396.
- WILKENING, JON & YU, JIA 2012 Overdetermined shooting methods for computing standing water waves with spectral accuracy. *Comput. Sci. and Disc.* **5**, 014017.
- WILLIAMS, J. M. 1981 Limiting gravity waves in water of finite depth. *Phil. Trans. R. Soc. Lond. A* **302(1466)**, 139–188.
- ZAKHAROV, VLADIMIR E., DYACHENKO, ALEXANDER I. & VASILIEV, OLEG A. 2002 New method for numerical simulation of nonstationary potential flow of incompressible fluid with a free surface. *European Journal of Mechanics B/Fluids* **21**, 283–291.
- ZAKHAROV, V. E. & DYACHENKOV, A. I. 1996 High-Jacobian approximation in the free surface dynamics of an ideal fluid. *Physica D* **98**, 652–664.